



Subduction–exhumation cycle recorded by calcite deformation microstructures: blueschist-facies metacarbonates and kinematic implications for deformation of the Meliata Unit (Western Carpathians)

Tomáš Potočný^{1,3} · Petr Jeřábek² · Dušan Plašienka¹

Received: 8 June 2022 / Accepted: 22 August 2023 / Published online: 6 September 2023
© The Author(s) 2023

Abstract

The Meliata Unit (Meliaticum) is a tectonic superunit of the Western Carpathians that incorporates the blueschists-facies Bôrka Nappe and the low-grade metasediments and polygenetic mélangé, Meliata Unit s.s., both occurring as scattered tectonic slices overlying the Gemeric Superunit. Calcitic marbles were sampled in a wide area within the Bôrka Nappe and blocks embedded in Jurassic oceanic sediments (Meliata Unit s.s.). Based on the microstructural evaluation and electron backscatter diffraction analysis (EBSD), the carbonates of the Bôrka Nappe experienced differential post-subduction P–T–D paths related to a collisional/exhumation setting following closure of the Neotethys-related “Meliata Ocean”. Variations in the calcite deformation microstructures were used to distinguish three principal microstructural groups. The first group (G1) contains large columnar and lobate calcite grains (≥ 1 mm) reflecting peak P–T conditions during subduction of the Meliata oceanic lithosphere. The second group (G2) exhibits dynamic recrystallization of the original G1 grains resulting in grain size reduction (< 0.5 mm) and shape-preferred orientation related to exhumation and formation of the accretionary complex. The third group (G3) shows a ‘foam’ microstructure with a uniform grain size (0.4–1 mm), sharp grain boundaries and triple junctions. The G3 microstructure may have been caused by a static recrystallization at elevated temperatures postdating the main deformation, and it is restricted to peripheries of the underlying Veporic metamorphic dome and probably is not associated with the Meliata sequences nor its tectono-metamorphic evolution. The corrected kinematic sections indicate dominantly ESE–WNW-trending lineations suggesting top-to-WNW kinematics of the Meliata subduction–exhumation process for G1 and G2 microstructures, and Gemeric–Veporic E–W orogen-parallel stretching for G3.

Keywords Meliata Unit · Metacarbonates · Microstructure · EBSD · Exhumation

Introduction

In collisional orogenic zones, the position of the fossil plate interface is represented by complexes characteristic of an oceanic suture. They include slices of ophiolites, high-pressure metamorphic rocks, a wide variety of syn-orogenic turbiditic flysch sediments with olistostrome bodies, and chaotic tectonic breccia masses of diverse composition known as mélanges (e.g., Hsü 1968, 1974; Ernst 1988; Festa et al. 2010). Another feature typical for the suture complexes is their complex and variable record of tectonic and metamorphic evolution (e.g., Wakabayashi 2015). Depending on the composition, position and velocity of the subduction and exhumation processes, certain rocks of the suture zone can record the initial stages of metamorphic and deformation processes associated with deep burial in the subduction channel (e.g., glaucophanites, eclogites). On the other hand, some rock units associated with

✉ Tomáš Potočný
potocny9@uniba.sk

Petr Jeřábek
jerabek.petr@natur.cuni.cz

Dušan Plašienka
dusan.plasienka@uniba.sk

¹ Department of Geology and Paleontology, Faculty of Natural Science, Comenius University, Mlynská Dolina, Ilkovičova 6, 842 15 Bratislava, Slovakia

² Institute of Petrology and Structural Geology, Faculty of Science, Charles University, Albertov 6, 128 43 Prague, Czech Republic

³ Department of Mineralogy, Petrography and Geochemistry, Faculty of Geology, Geophysics and Environmental Protection, AGH-University of Science and Technology, Al. Mickiewicza 30, 30-059 Krakow, Poland

suture zones were completely uninvolved in the subduction and they rather reflect low-grade metamorphic transformations and deformation within the accretionary wedge. While deeply subducted complexes often provide valuable information about increasing temperature–pressure conditions during burial and subsequent exhumation associated with cooling and decompression, the shallowly subducted units may record a simple pressure–temperature and strain path (Wakabayashi 2015).

Calcite-bearing rocks, such as limestones, represent an important lithology involved in subduction–accretionary complexes as they show plastic deformation even at relatively low temperature–pressure conditions (e.g., Bestmann et al. 2000; Herwegh and Pfiffner 2005). More importantly, deformation in calcitic metacarbonates often leads to localization as a result of increasing strain (Oesterling et al. 2007), increasing strain rate (Rogowitz et al. 2014) or presence of impurities (Herwegh and Kunze 2002; Herwegh and Berger 2004). As a consequence, the earlier deformation of metacarbonates can be revealed by microstructural studies allowing for distinction of subducted and non-subducted portions of accretionary complexes, as well as for documentation of individual stages of the subduction–exhumation process. The subduction stages and high-pressure conditions in calcite microstructures can be identified thanks to pressure-induced transformation of calcite to aragonite and its later back-reaction to pseudomorphs of columnar calcite (Brady et al. 2004; Seaton et al. 2009; Gerogiannis et al. 2021; Aravadinou et al. 2022). On the other hand, formation of mylonite microstructures typically accompanies extreme deformation during exhumation (e.g., Herwegh and Pfiffner 2005).

The present work is devoted to marbles of the high-pressure metamorphosed Bôrka Nappe and blocks in low-grade *mélange*—Meliata Unit s.s., which are a parts of the subduction–accretion complex of the Triassic–Jurassic, Neotethys-related oceanic domain, commonly referred to as the “Meliata Ocean”, remnants of which are preserved in the Western Carpathians. The imbricated Meliatic complexes occur as a structurally complex nappe stack overriding the Gemic Unit (Gemicum) of the Central Western Carpathians (e.g., Plašienka et al. 2019). The sampled metacarbonates come from different occurrences of the Meliata Unit subduction–accretion complex and as such reveal very different microstructures. An attempt has been made to correlate the individual sites in terms of their tectono-metamorphic record.

Geological setting

Based on a regional tectonic division of the Western Carpathians (Plašienka 2018), the Meliata Superunit (Meliaticum) is placed in the contact area of the Central (CWC) and

Internal Western Carpathians (IWC). The southern zones of the CWC are formed by the thick-skinned Veporic and overlying Gemic complexes (Fig. 1). The structurally lower Vepor Unit (Veporicum) is a crustal-scale sheet composed of the pre-Alpine basement and its Upper Paleozoic to Mesozoic sedimentary cover, both affected by the Eo-Alpine (Cretaceous) greenschist- to lower amphibolite-facies metamorphism (e.g., Janák et al. 2001; Jeřábek et al. 2007, 2012). This metamorphism was associated with burial of the Vepor Unit during overthrusting by the Gemic thick-skinned sheet from the south followed by extensional top-to-east unroofing of the Vepor Unit from below the Gemic sheet (Janák et al. 2001; Jeřábek et al. 2012; Bukovská et al. 2013; Novotná et al. 2015; Vojtko et al. 2016). The contact zone between the two major units, in terms of both thrusting and extension events, is represented by the so-called Lubeník shear zone, which in the studied area shows WSW–ENE strike, changing eastward to N–S to NNW–SSE direction (Fig. 1). Bedding and metamorphic foliations in the SE part of the Vepor Unit are south or east-dipping, while the pervasive stretching lineation remains constantly plunging to the ENE to E (Plašienka 1993; Janák et al. 2001; Jeřábek et al. 2012). This structure represents regional axial plunge of the Veporic dome below Gemic units which was later reactivated by significant transtensional movements (e.g., Novotná et al. 2015; Potočný et al. 2020).

The basement of the overlying Gemic Unit is composed of polymetamorphic greenschist-facies Lower Paleozoic metavolcano-sedimentary complexes, which are covered by low-grade Lower Paleozoic to Triassic deposits (Vozárová and Vozár 1988; Vozárová 1996). The general structure of the Gemic Unit shows a development of a large-scale cleavage fan affecting the pre-Alpine basement and its Upper Paleozoic to Mesozoic sedimentary cover. This structure reflects the Eo-Alpine northward thrusting of the Gemic sheet over the Vepor Unit followed by transpression along the Lubeník shear zone (Lexa et al. 2003). The Meliatic, Turnaic and Silicic cover nappe systems, which represent the IWC, form a nappe pile overlying the Gemic Unit (Fig. 1).

The Meliata Superunit consists of four different, but interrelated imbricated complexes (Plašienka et al. 2019): (1) high-pressure and low-temperature (HP–LT) metamorphosed Bôrka Nappe in the lowest structural position (Permian–Triassic, possibly also Jurassic; e.g., Faryad 1995a, b; Mello et al. 1998); (2) ophiolitic *mélange* with blocks of igneous and sedimentary rocks (Triassic–Jurassic; Ivan 2002; Faryad et al. 2005); (3) a complex of weakly metamorphosed Jurassic shales, turbiditic sandstones and radiolarites with olistostrome bodies of Triassic carbonates and basalts (Meliata Unit s.s.; e.g., Mock et al. 1998; Árkai et al. 2003); and (4) polygenetic *mélange* at the interfaces of the previous complexes containing fragments of the Bôrka Nappe, ophiolites and the low-grade Jurassic clastics (e.g., Ivan and

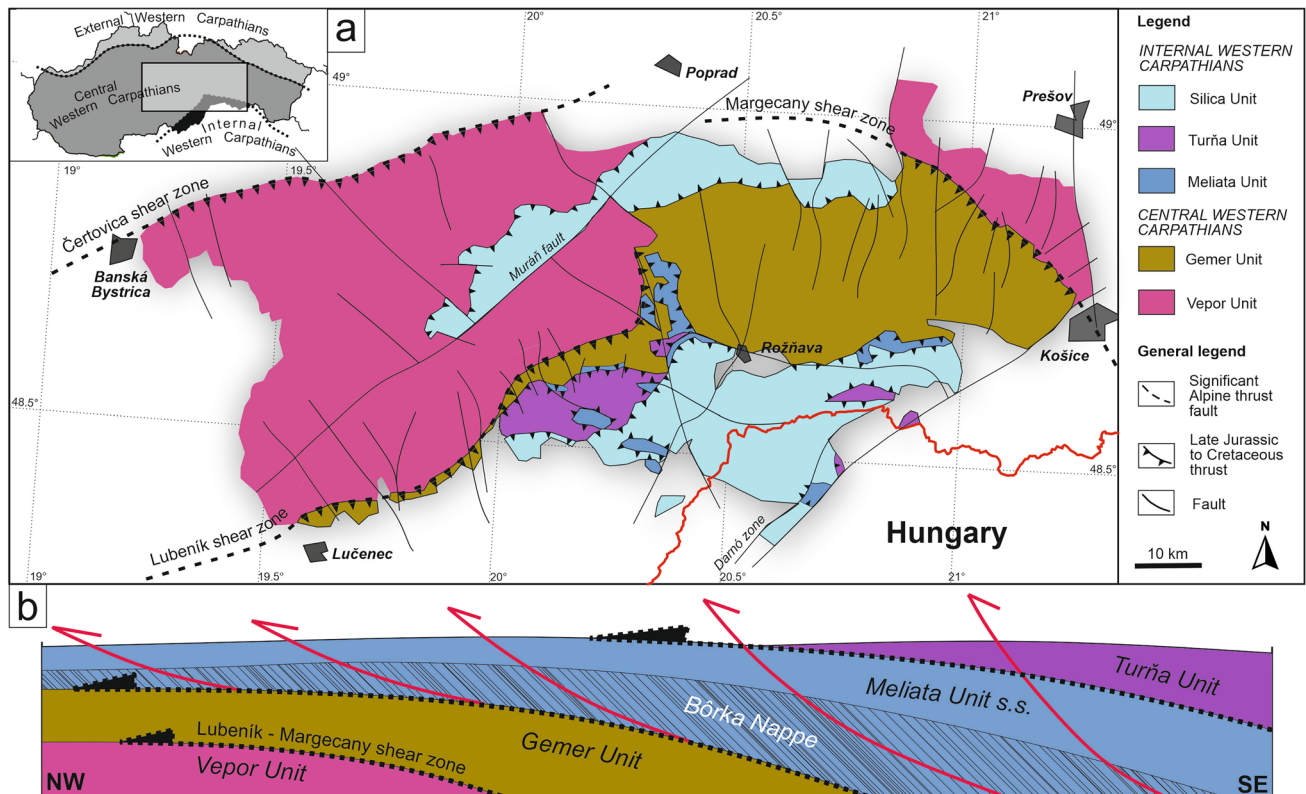


Fig. 1 Investigated part of the Western Carpathians in Slovakia: **a** tectonic sketch; **b** schematic profile with the main structural elements, red arrows—out-of-sequence thrusting

Méres 2009; Putiš et al. 2011, 2019; Plašienka et al. 2019). The overlying Turňa Unit (Turnaicum) is in a close relationship with the Meliata Unit. They jointly form an amalgamated, imbricated and folded accretionary complex overriding the Gemer Unit (Lačný et al. 2016; cf. Fig. 1). The low-grade Turňa Unit includes the Upper Paleozoic to Lower Triassic clastic deposits, but especially the Middle–Upper Triassic deep-water limestones. The unmetamorphosed Silica Nappe (Silicicum) in the uppermost structural position is composed of the Permian–Lower Triassic evaporites and clastic sediments, but is dominated by a massive complex of Middle–Upper Triassic platform carbonates (e.g., Mello 1975; Reichwalder 1982). Jurassic sediments are preserved in few places only.

The HP–LT metamorphosed Bôrka Nappe, the main object of our study, represents a tightly imbricated complex of metasedimentary and metavolcanic rocks. Due to its metamorphic overprint, no fossils have been preserved in this nappe and therefore its stratigraphic assignment is based only on lithological correlation. The period of the Permian to Early Triassic is represented by clastic continental metasediments and acid metavolcanites (Mello et al. 1998). This lower lithological complex is very similar to the underlying cover of the Gemer Unit, but differences can be observed in

the degree and character of deformation and metamorphism (e.g., Vozárová et al. 2019). The upper lithological complex of the Bôrka Nappe includes probably Anisian light massive metacarbonates containing coeval basic volcanoclastics and lava flows in the upper parts (named by Mello et al. 1998 as the Dúbrava Formation), which are often transformed to glaucophanites. The overlying complex of phyllites, metacherts and carbonate breccias is of the Late Triassic to possibly Jurassic age.

There are several palaeotectonic reconstructions for zones associated with the Meliatic complexes inferring their relationship to the Middle Triassic opening and subsequent Late Jurassic closure of the “Meliata Ocean” (Kozur 1991; Kovács 1992; Rakús 1996; Channell and Kozur 1997; Csontos and Vörös 2004; Haas et al. 1995; Less 2000; Stampfli and Kozur 2006; Schmid et al. 2008; Dallmeyer et al. 2008; Missoni and Gawlick 2011; Kövér et al. 2018; Szives et al. 2018; Plašienka et al. 2019). These concepts assume different position of the Meliata Ocean: (1) as an independent back-arc basin inboard the European margin related to the northward subduction of Palaeotethys; (2) as the NW-ward wedging-out embayment of the Neotethys Ocean; (3) as a remnant oceanic basin in front of obducted Vardar ophiolite nappes, or (4) merely as a facies zone of the Neotethyan

distal passive margin. To avoid misunderstandings, the term “Meliata Ocean” in parentheses is used throughout this paper, which means that no genetic connotation of this oceanic domain is given and no its relationships to other Neotethyan domains are treated here.

The former northern European margin of the “Meliata Ocean” became the lower tectonic plate during the Jurassic subduction, when its southern Adria-related margin was transformed from a passive to an active one with the Meliatic complexes squeezed in between. Middle Anisian (Pelsonian) rifting of the “Meliata Ocean” is confirmed by deep-water pelagic sediments filling the cracks within the disintegrating Lower Anisian platform carbonates (e.g., Kozur and Mock 1973). Subsequent passive margin subsidence was associated with the expansion of the “Meliata Ocean”. The convergent stage is characterized by sedimentation of the distal turbidites and olistostrome bodies derived from the active margin setting. After the Meliatic oceanic lithosphere was fully subducted, the former European passive margin (the CWC Gemeric and the future Bôrka Nappe as its distal fringe) was dragged into the subduction and underwent HP–LT metamorphism characterized by mineral assemblages formed at 460–520 °C and 1–1.5 GPa (Faryad 1995a, b; Faryad and Hoinkes 1999; Nemeč et al. 2020). Peak of the high-pressure metamorphism in metasediments was dated by $^{40}\text{Ar}/^{39}\text{Ar}$ method to approximately 160–150 Ma (e.g., Faryad and Henjes-Kunst 1997; Dallmeyer et al. 2008). However, these data are limited to the southernmost parts of the Bôrka Nappe, where it is mostly covered by the overlying tectonic units. The external (north-western) parts of Bôrka Nappe overlying the Gemer Unit reached lower metamorphic conditions of greenschist and/or transitional greenschist–blueschist facies (Ivan et al. 2009; Putiš et al. 2012). Lower Cretaceous exhumation has been documented by the retrograde metamorphism of HP rocks under greenschist-facies conditions, structural and thermochronological data (e.g., Faryad 1999; Dallmeyer et al. 2008; Putiš et al. 2009, 2014, 2015, 2019; Potočný et al. 2020; Nemeč et al. 2020).

Sampling and methods

Field work and sampling aimed to cover the largest possible number of occurrences of the Bôrka Nappe and the Meliata Unit s.s. (Fig. 2; Table 1). Sampling was focused on lithologically similar, pale to white massive metacarbonates, especially calcitic marbles designated as the Honce Limestone in Slovakia. Altogether 27 samples were collected. The thin sections were made perpendicular to the main metamorphic foliation and parallel to the lineation as observed in the field (see Table 1 for foliation and lineation measurements). Samples without visible

lineation, were cut (thin sections) perpendicular to foliation and parallel to the foliation maximum dip (MD measurements in Table 1). The photomicrographs and stereographic projections of crystallographic orientations are presented in sections parallel to the measured lineation and perpendicular to the measured foliation. Sample investigation was focused on differences in the rock composition and various observable microstructure features.

To better understand the evolution of the microstructures, 12 selected samples were analyzed in Cathodoluminescence (CL) mode. A “hot-cathode” (Walker and Burley 1991) in the CL-Lab of Department of Geosciences at the University of Fribourg (Switzerland) was used to investigate the cathodoluminescence of specific features of the calcite microstructures. An acceleration voltage of 19 kV was applied.

Based on the microstructural criteria, eight representative samples were selected for the Electron Backscatter Diffraction (EBSD) analysis performed at the Institute of Petrology and Structural Geology of the Faculty of Science, Charles University in Prague (Czech Republic). EBSD data were acquired using the scanning electron microscope Tescan Vega equipped with NordLys Nano detector (Oxford Instruments), in point-beam mode at 20 kV and 7 nA, and a step size between 5 and 15 μm . The EBSD data were collected using the AZtec software (Oxford Instruments) and processed with Matlab toolbox MTEX 4.5.1. (Hielscher and Schaeber 2008). This method was used to determine numerous structural and textural aspects as phase, crystallographic orientation of grains, grains reconstruction, twins recognition and their removal, grain size distribution, and shape-preferred orientation. The grain diameter was determined from reconstructed grain maps as equal area diameter, i.e., the diameter of a circle with area that is equivalent to the grain. The resulting grain size of each sample is presented as curves connecting peaks of grain diameter histogram. The grain maps based on EBSD measurements are shown after twin lamellae removal. Crystallographic preferred orientation (CPO) data are plotted as orientation distribution function (ODF) calculated from all measured points in the respective EBSD maps by Fourier method with de la Vallée Poussin kernel and a half width of 16° . Crystallographic and shape fabrics show preferred orientations with respect to a sample reference system. The resulting crystallographic data are shown in the equal area upper hemisphere projection pole figures for {0001}, [11-20], {10-14}, {01-12}, {01-18} planes and directions that are commonly used to characterize texture of calcitic rocks. Shape preferred orientation (SPO) was illustrated as rose diagram for each sample in pole figures of {01-18}.

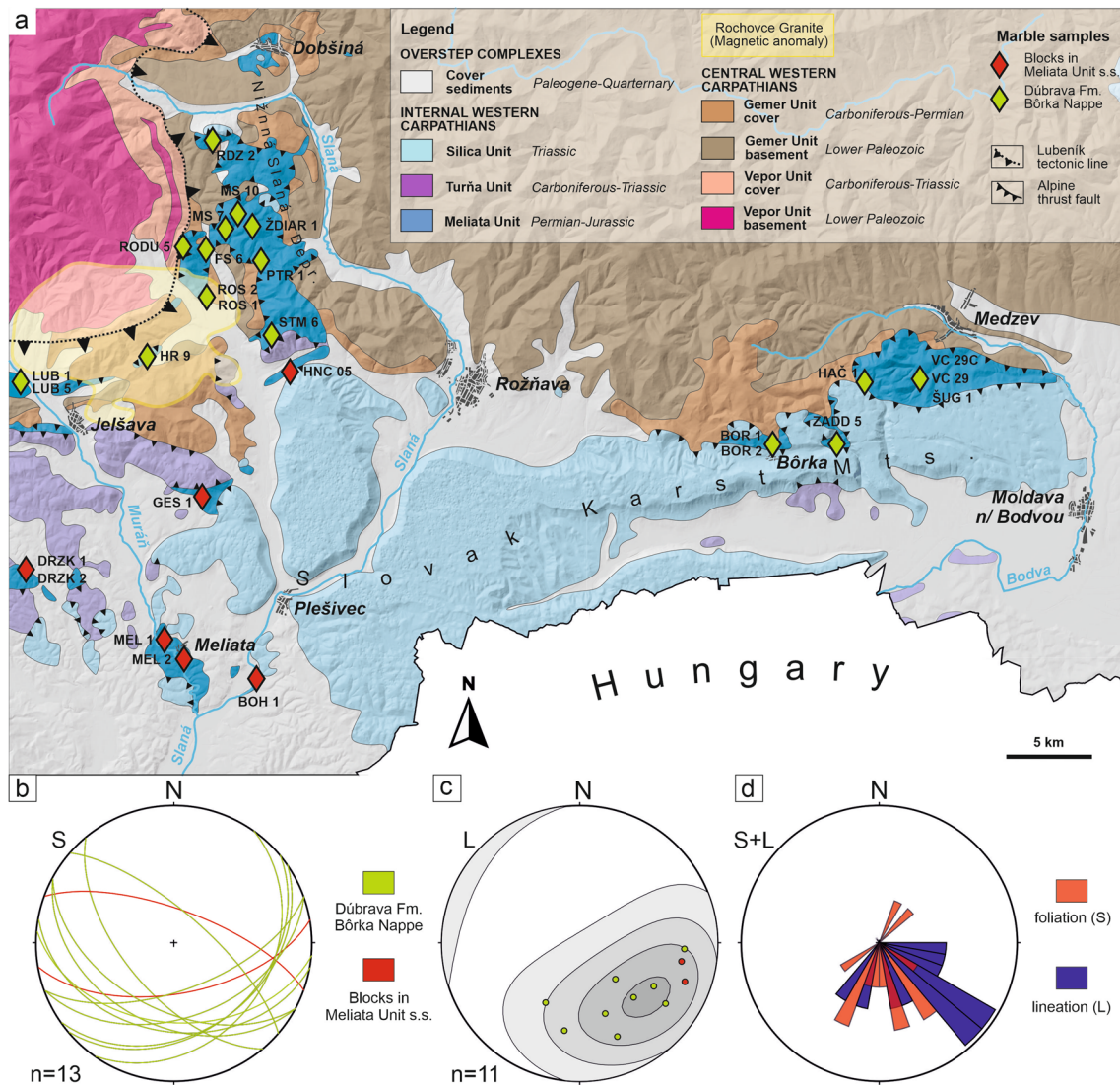


Fig. 2 Tectonic sketch map, modified after Bezák et al. (2004), of the investigated area with stereograms of the main structural elements measured in the field: **a** tectonic map with occurrences of the Meliata

Unit and sample locations; **b** orientation of the foliation planes of oriented samples; **c** orientation of the lineation of oriented samples; **d** rose diagram of the structural elements

Results

Altogether 27 samples (Table 1) were collected at 21 localities in a wide area of the Meliata Unit (Fig. 2). Two main groups can be distinguished from structural point of view as (1) metacarbonates in association with basic volcanics and metasediments of the Bôrka Nappe, and (2) bodies of metacarbonates (olistoliths and/or tectonic slices) in polygenetic mélange of the Meliata Unit s.s. (Fig. 2a). All collected samples are represented by light, white or yellowish-colored crystalline metacarbonate, rarely with a tint of different color caused by impurities. Primary sedimentary layering of metacarbonates of the first group is observed as compositional banding related to contribution of volcanic material (Fig. 3). The layering

is typically subparallel to the metamorphic foliation S_{0-1} (Fig. 3) which usually shows a weak lineation L_1 . Locally, the mylonitic foliation S_2 transposes S_{0-1} (Fig. 3b), or secondary axial-planar cleavage S_2 is developed in northward-facing tight asymmetric folds typical of the Bôrka Nappe (Fig. 3c). In places without clear overprinting relations, the S_{0-1} and S_2 are macroscopically indistinguishable, therefore, only S and L measurements are indicated for the studied samples (Table 1). The metamorphic foliation S of the collected samples is generally gently to moderately SE–SW dipping (Fig. 2b, d) and the lineation L mostly plunges to the SE (Fig. 2c, d). The metacarbonate blocks of the second group occur as large bodies embedded in soft Jurassic sediments of the Meliata Unit s.s. (Fig. 3d). With the exception of two samples (Table 1), these carbonates

Table 1 Investigated samples, their GPS, positions and characteristics (measurement of oriented samples: S = foliation; L = lineation; MD = maximum dip)

Sample	GPS (WGS 84)	Position	Mineral composition	Oriented sample
MEL 1	N48.517008 E20.324691	Meliata Unit s.s.	<i>Cal+Dol</i>	
MEL 2	N48.512410 E20.330896	Meliata Unit s.s.	<i>Cal+Dol</i>	
DRZK 1	N48.548337 E20.220391	Meliata Unit s.s.	<i>Cal+Dol</i>	
DRZK 2	N48.545695 E20.224864	Meliata Unit s.s.	<i>Cal+Dol</i>	
MS 7	N48.727736 E20.339937	Dúbrava Fm.	<i>Cal+Ms, Qz, Ab, Ilm</i>	
HAČ 1	N48.668891 E20.833704	Dúbrava Fm.	<i>Cal+Qz</i>	<i>S230/60 L320/20</i>
BOH 1 ^a	N48.505874 E20.386655	Meliata Unit s.s.	<i>Cal+Dol</i>	<i>S170/60 L110/20</i>
HNC 5 ^a	N48.657294 E20.394208	Meliata Unit s.s.	<i>Cal+Qz</i>	<i>S20/70 L100/26</i>
GES 1	N48.587896 E20.346326	Meliata Unit s.s.	<i>Cal+Dol</i>	
ŠUG 1 ^a	N48.673103 E20.874906	Dúbrava Fm.	<i>Cal+Dol, Ms, Qz</i>	<i>S41/72 L125/25</i>
ŽDIAR 1	N48.731328 E20.364704	Dúbrava Fm.	<i>Cal+Dol, Qz</i>	
BOR 1 ^a	N48.637285 E20.764396	Dúbrava Fm.	<i>Cal+Dol</i>	<i>S160/62 L135/60</i>
BOR 2	N48.638715 E20.763763	Dúbrava Fm.	<i>Cal+Dol, Ab</i>	<i>S160/45 L160/45</i>
ZADD 5	N48.638127 E20.811244	Dúbrava Fm.	<i>Cal</i>	
RODU 5	N48.714383 E20.313608	Dúbrava Fm.	<i>Cal+Qz, Dol</i>	
PTR 1	N48.715146 E20.361429	Dúbrava Fm.	<i>Cal+Qz</i>	
VC 29 ^a	N48.669312 E20.874925	Dúbrava Fm.	<i>Cal+Qz</i>	<i>S140/35 L120/33</i>
ROS 1 ^a	N48.692887 E20.333880	Dúbrava Fm.	<i>Cal+Qz, Ms, Dol, Ilm</i>	<i>S208/40 L158/28</i>
ROS 2 ^a	N48.693058 E20.332277	Dúbrava Fm.	<i>Cal+Qz, Dol</i>	<i>S208/50 L210/49</i>
LUB 1	N48.648782 E20.196047	Dúbrava Fm.	<i>Cal+Dol</i>	<i>S185/42 MD185/42</i>
LUB 5	N48.649058 E20.187635	Dúbrava Fm.	<i>Cal+Chl, Dol</i>	
STM 6	N48.672614 E20.377407	Dúbrava Fm.	<i>Cal+Dol</i>	
HR 9 ^a	N48.661829 E20.285482	Dúbrava Fm.	<i>Cal+Chl, Ilm, Qz, Ab</i>	<i>S190/36 MD190/36</i>
FS 6 ^a	N48.715119 E20.232087	Dúbrava Fm.	<i>Cal+Chl, Dol</i>	<i>S145/35 L93/25</i>
VC 29C ^a	N48.669312 E20.874925	Dúbrava Fm.	<i>Cal+Qz</i>	<i>S125/30 L135/44</i>
MS 10	N48.731402 E20.345607	Dúbrava Fm.	<i>Cal+Qz</i>	
RDZ 2	N48.773382 E20.331016	Dúbrava Fm.	<i>Cal + Qz, Ms, Ab, Ilm</i>	

^aSamples studied by electron backscatter diffraction analysis (EBSD)

are usually without any significant macroscopic structural elements.

Calcite deformation microstructures

The studied samples were divided into three groups based on differences in calcite microstructures. The distinctive features are based on microstructural criteria including degree of recrystallization, recrystallization character and size and shape of grains. Figure 4 summarizes different microstructural features of the studied metacarbonates in relation to the observed deformation fabrics. In principle, the microstructures show an earlier coarse-grained microstructure with relics of columnar calcite that was overprinted by recrystallization to various extent.

Group 1

Group 1 (G1) microstructure is characterized by large grain size (> 1 mm; Figs. 5a–f, 6). However, two distinct microstructural features further split this group into G1A and G1B

microstructures. The main feature of G1A (Fig. 5a–c) is an occurrence of the columnar calcite, while lobate shapes of large calcite grains determine the G1B (Fig. 5d–f). The G1A grains are characterized by elongate shapes with usually strong intragranular deformation in the form of columnar subgrains and undulose extinction (Fig. 5). The columnar microstructure without evidence for subsequent recrystallization is rarely well preserved, as recrystallization of calcite is observed in almost all samples with columnar calcite microstructure. The G1B microstructure is characterized by typical irregular boundaries of big calcite grains that do not show any shape-preferred orientation (Fig. 5d–f). Similar to the columnar calcite microstructure, the lobate calcite grains shown intense intragranular deformation.

The large calcite grains of G1 show variable forms of twin lamellae, from very thin to thick, curved, and often recrystallized lamellae. Such twins correspond to geometric types II–IV (~ 200 °C) of Burkhard (1993). Three coarse-grained marble samples from G1 were investigated by EBSD. Sample BOR 1 and ŠUG 1 show similar texture with *c*-axes and poles to *e*-planes clustering in a broad single



Fig. 3 Phototable of Meliatic metacarbonates in the field: **a** foliation S_{0-1} in Bôrka Nappe metacarbonates visible in an old quarry (Roštár—ROS 02); **b** strong tectonic overprint of mixture of carbonate and volcanic material with rotated σ and δ clasts pointing to

generally top-to-NW shearing (Šugov Valley—VC 29); **c** folded metacarbonate strata interlayered by volcanic material (Hrádok—HR 9); **d** block of marble embedded in Jurassic deep-water sediments (Držkovce—DRZK 01)

point maximum perpendicular to the reference foliation plane and a -axes showing a broad single girdle subparallel to foliation (Fig. 5g, h). The maximum concentration of a -axes is subparallel and slightly oblique to the measured lineation for sample ŠUG 1 and BOR 1, respectively. SPO of reconstructed grains in these samples is subparallel to the foliation. Sample HNC 5 shows a single girdle of c -axes and poles to e -planes oblique to the macroscopic foliation and subparallel to the grain SPO (Fig. 5i).

Group 2

Large calcite grains of G1 are often overprinted by recrystallization which, with increasing overprint intensity, can be distinguished as the separate Group 2 (G2) microstructure (Fig. 7). Augmenting stages of recrystallization are accomplished by the development of completely recrystallized mylonites (Fig. 7c, d). G2 grains are characterized by relatively small size of $<500\ \mu\text{m}$ (Fig. 6) showing either no signs of shape-preferred orientation in less recrystallized samples, or strong shape-preferred orientation

in calcitic mylonites (cf. Fig. 7c, d). Results from the cathodoluminescence (CL) imaging allowed to distinguish two separate generations of calcite associated with G1 and G2 microstructures (Fig. 8). Dark CL of the first generation calcite (Cal1) is associated with coarse-grained G1 microstructure, while brighter CL of the second calcite generation (Cal2) is associated with fine-grained G2 (Fig. 8a–d). The CL images also manifest different degree of transformation of Cal1 into younger Cal2 and consequently degree of recrystallization of G1 by G2 (Fig. 8).

In addition, G2 calcite grains show multiple sets of mostly very thin twin lamellae, such as the geometric type II (150–300 °C) described by Burkhard (1993). One mylonite marble sample VC 29 analyzed by EBSD is characterized by a single maximum of c -axes and poles to e -planes perpendicular to the reference foliation and by a broad single girdle of a -axes subparallel to foliation with their maximum concentration slightly oblique to the measured lineation (Fig. 7g). The grain SPO forms foliation that is oblique to the reference foliation plane.

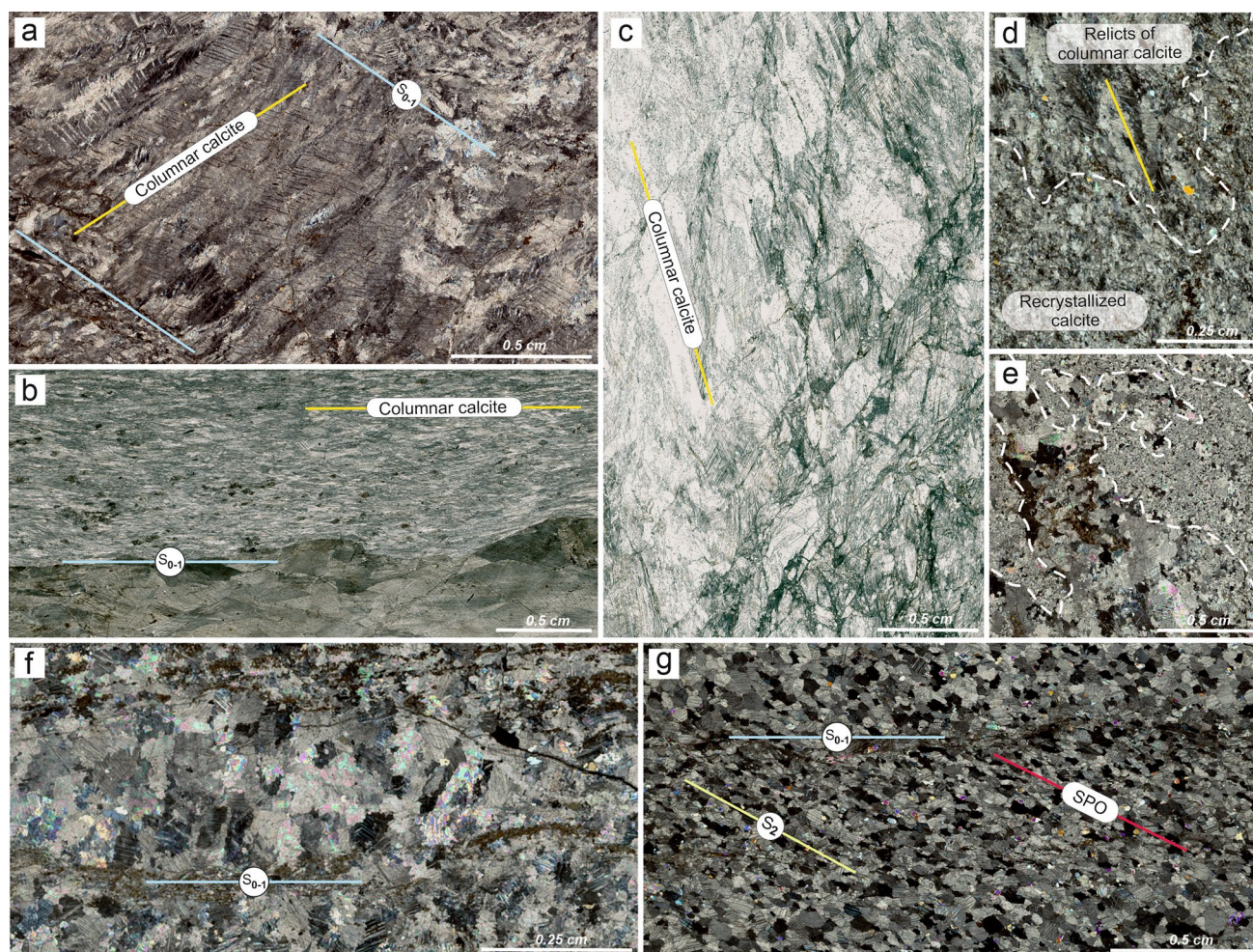


Fig. 4 Photomicrographs of different calcite microstructures of the Meliatic metacarbonates: **a** columnar calcite oblique to the foliation as pseudomorphs after aragonite (Hačava—HAČ 1); **b** columnar calcite parallel to foliation (Bôrka—BOR 2); **c** brittle overprint of HP metacarbonate with columnar calcite (Honce—HNC 5); **d** relict of

a columnar calcite in recrystallized marble (Ždiar Hill—ŽDIAR 1); **e** zones of different grains size (Bohúňovo—BOH 1); **f** calcite marble recrystallized by Grain Boundary Migration mechanism (Šugov Valley—ŠUG 1); **g** recrystallized and annealed? microstructure with SPO of calcite grains oblique to foliation (Hrádok—HR 9)

Group 3

Group 3 (G3) of calcite microstructures is distinguished by a specific microstructure resembling the completely recrystallized so-called foam microstructure (Fig. 9a–c). Calcite grains of G3 are mostly equi-axed and of similar size (0.5–1 mm in Fig. 6) and often show relatively straight boundaries (Fig. 9). Similarly, to the Cal1 grains of G1, the CL of G3 grains is also dark (Fig. 8). G3 calcite grains contain deformation twins, like geometric type I or II suggesting temperatures between 150 and 300 °C (Burkhard 1993). Regional occurrence of the G3 microstructure is limited to the surroundings of the Lubeník shear zone marking the major tectonic contact between the Gemic and Veporic units (Fig. 11).

Four samples from G3 were selected for EBSD analysis (Fig. 9d–g). Samples ROS 1 and HR 9 show a single maximum of *c*-axes and *e*-axes perpendicular to the reference foliation and by a broad single girdle of *a*-axes subparallel to foliation (Fig. 9d, e). The maximum of *a*-axes in both samples is located close to the *y*-orientation of the finite strain ellipsoid, i.e., perpendicular to the measured lineation. Sample FS 6 shows a single girdle of *c*-axes and poles to *e*-planes perpendicular to the reference foliation and by a broad single girdle of *a*-axes subparallel to foliation with their maximum concentration subparallel to the measured lineation (Fig. 9f). Analogously to the G1 sample HCN 5 (Fig. 5i), the sample ROS 2 shows a single girdle of *c*-axes and *e*-axes slightly oblique to the macroscopic foliation and subparallel to the grain SPO (Fig. 9g).

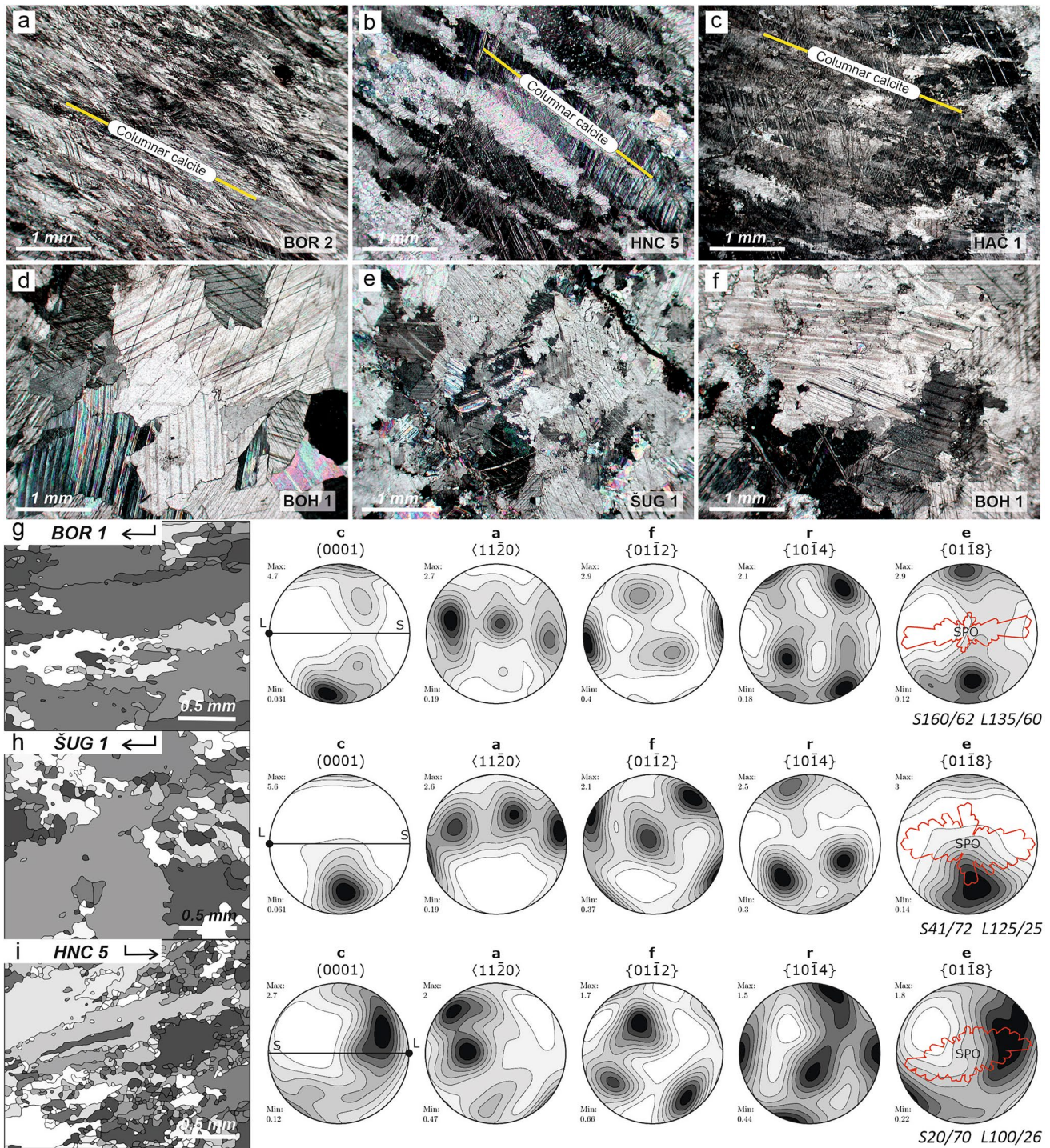


Fig. 5 Microphotographs of Group 1 calcite microstructures in cross-polarized light: **a** columnar calcite; **b–c** recrystallized columnar calcite; **d–f** lobate calcite crystals; **g–i** EBSD maps of reconstructed grains, arrows indicate top of the sample and lineation plunge, the associated pole figures show CPO plotted with respect to the sample

reference frame (measurement of foliation S and lineation L is also indicated), foliation trace S and lineation orientation L (identical for all pole figures) are shown in the c-axis pole figure, the SPO of reconstructed grains is shown as rose diagram in the e-planes pole figure

Fig. 6 Histogram of the distribution of microstructural groups based on the grain diameter

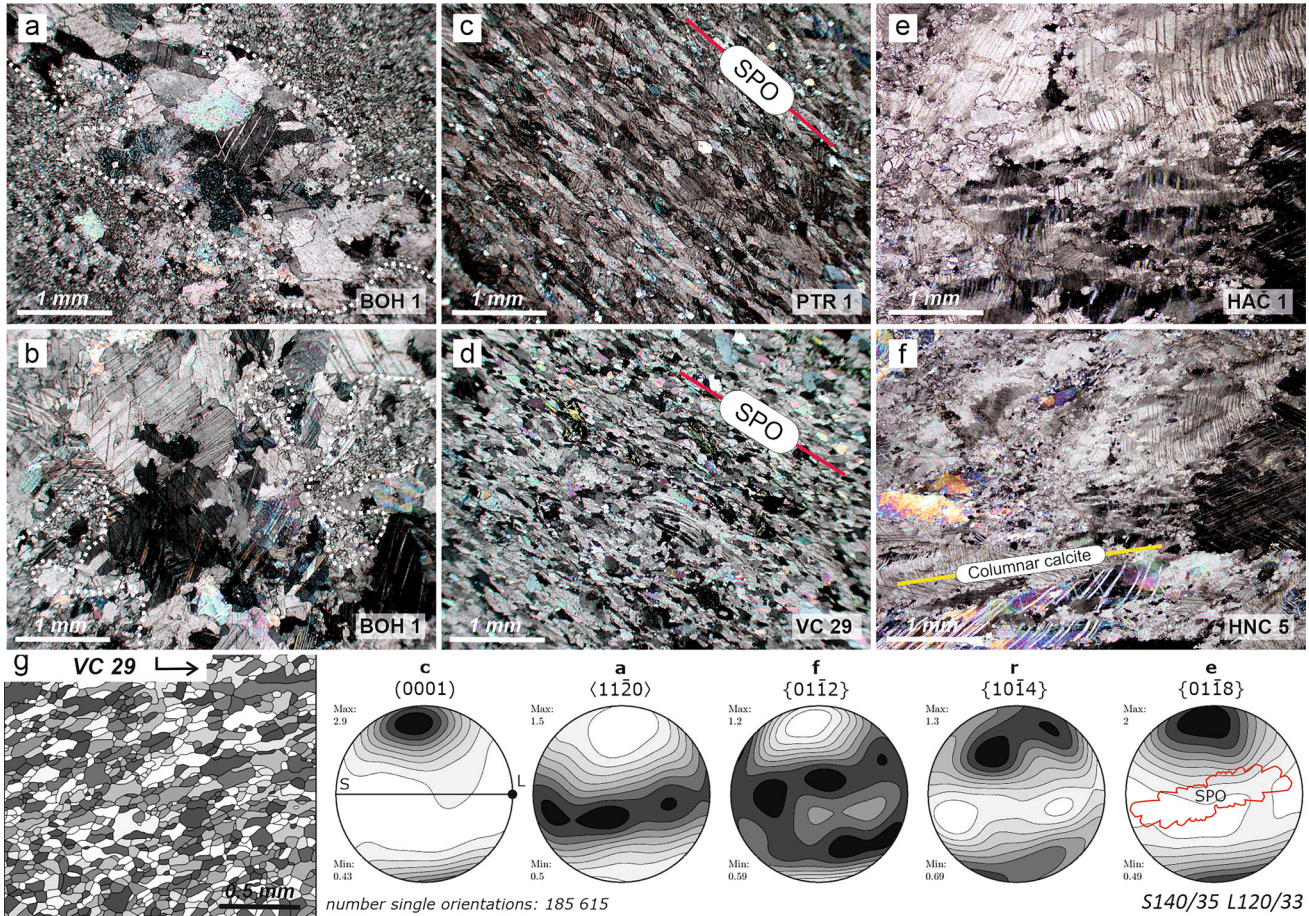
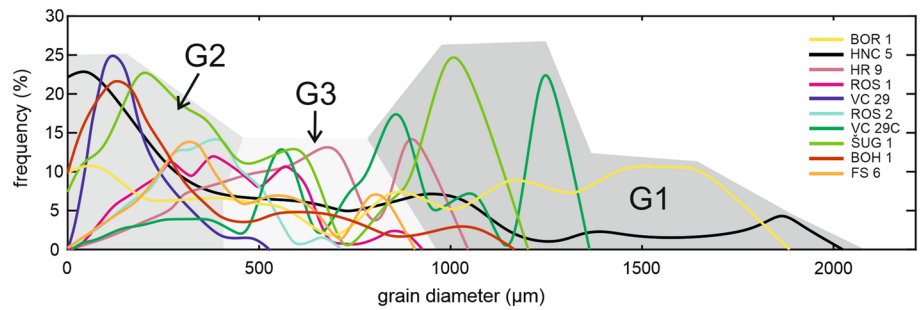


Fig. 7 Group 2 calcite microstructures; photomicrographs in cross-polarized light: **a**, **b** microstructure with zones of grain size reduction without SPO; **c**, **d** microstructure of mylonitic marbles with strong SPO and grain size reduction; **e**, **f** microstructure of low-temperature brittle deformation with relics of columnar calcite; **g** map of reconstructed grains, arrow indicates top of the sample and lineation

plunge, the associated pole figures show CPO plotted with respect to the sample reference frame (measurement of foliation S and lineation L is also indicated), foliation trace S and lineation orientation L (identical for all pole figures) is shown in the *c*-axis pole figure, the SPO of reconstructed grains is shown as rose diagram in the *e*-planes pole figure

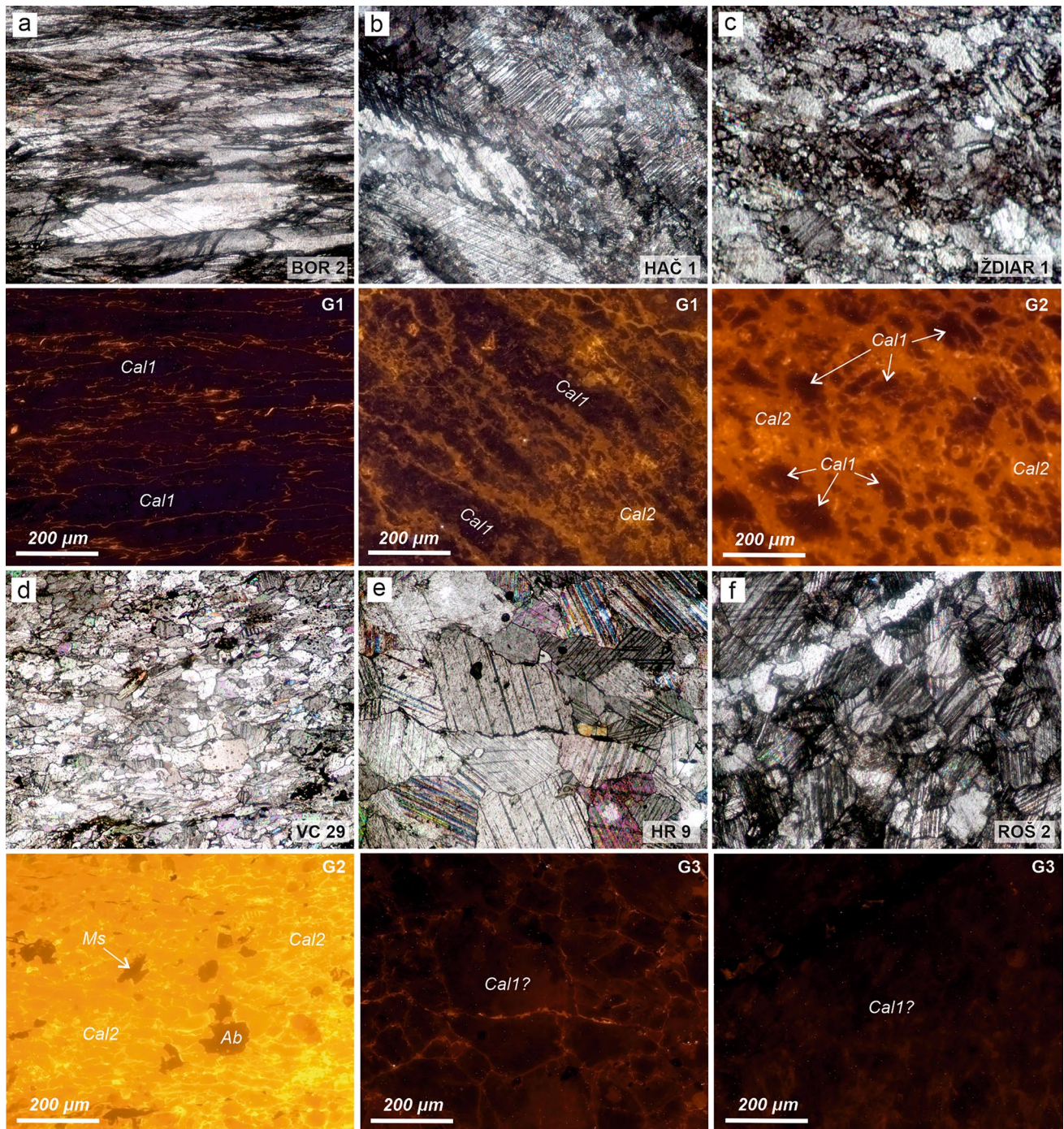


Fig. 8 CL images of two calcite generations: **a** microstructure with columnar calcite—Cal1 (dark CL, non-luminescent); **b** columnar Cal1 (dark CL, non-luminescent) with new recrystallized Cal2 domains (brownish-dark orange CL; **c** recrystallized Cal2 (dark

orange-bright orange CL) with relicts of Cal1 (dark CL, non-luminescent); **d** completely recrystallized mylonite with Cal2 (bright orange-yellow CL); **e, f** foam texture of calcite with no or very weak luminescence (dark-dark brown CL)

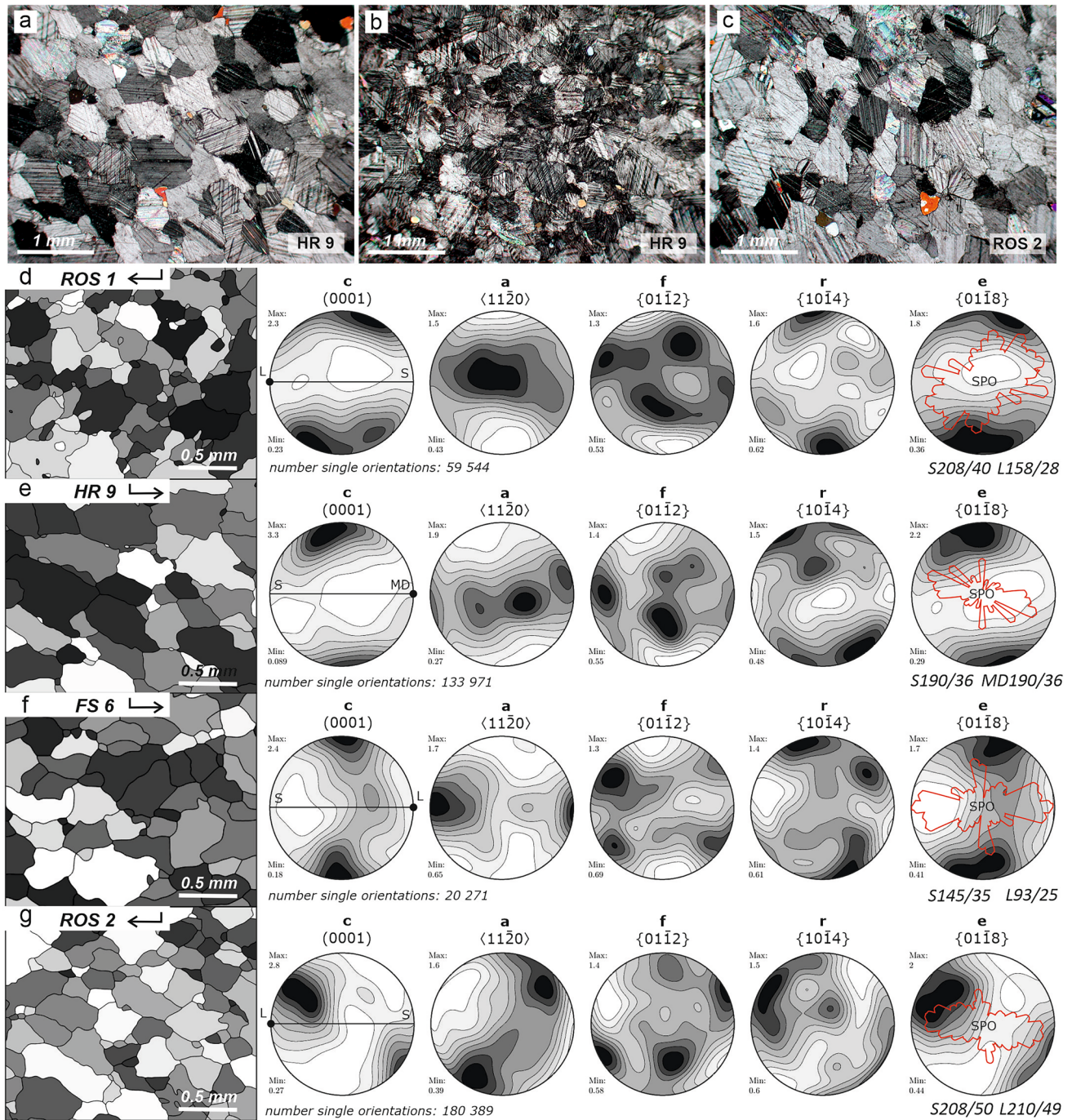


Fig. 9 Group 3 calcite microstructures; photomicrographs in cross-polarized light: **a**, **c** foam microstructure; **d**, **g** maps of reconstructed grains, arrows indicate top of the sample and lineation plunge, the associated pole figures show CPO plotted with respect to the sample

reference frame (measurement of foliation S and lineation L is also indicated), foliation trace S and lineation orientation L (identical for all pole figures) is shown in the c-axis pole figure, the SPO of reconstructed grains is shown as rose diagram in the e-planes pole figure

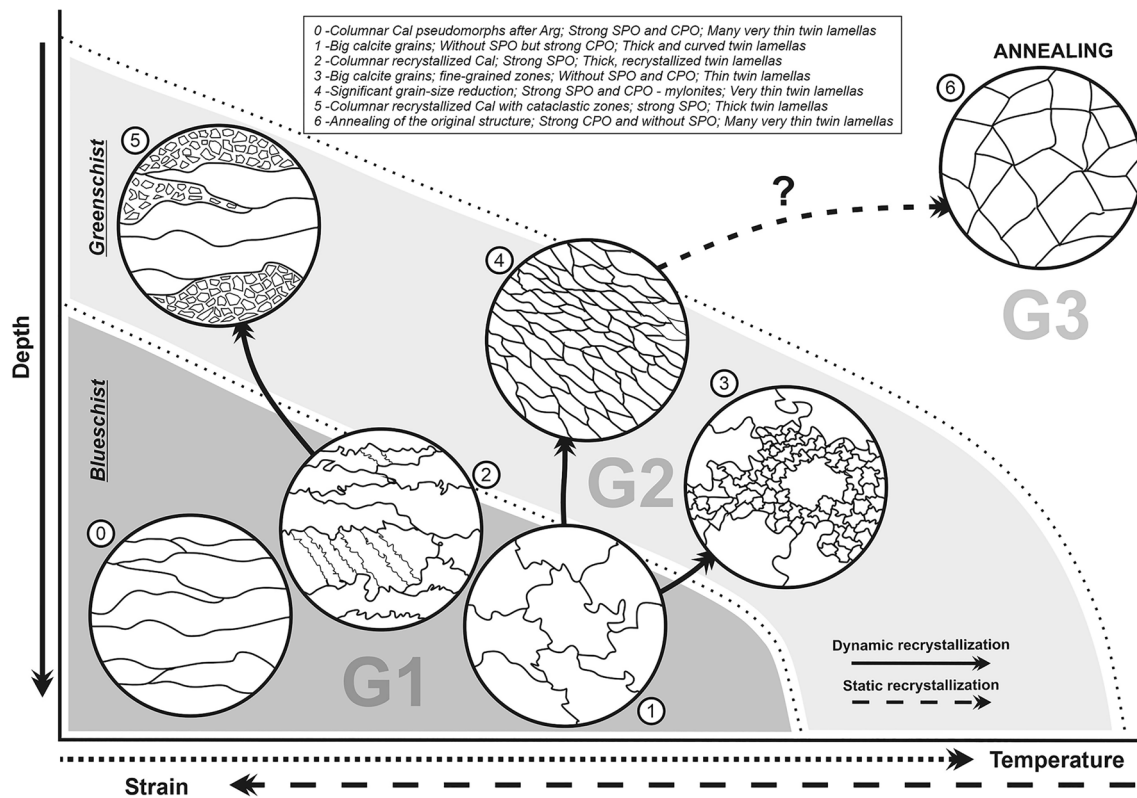


Fig. 10 Summary of the observed calcite microstructures of the Meliatic metacarbonates and their tentative evolution in the P–T space

Discussion

Calcite microstructures in the context of regional tectonic events

Based on the character of observed calcite microstructures (Fig. 10), their spatial occurrence (Fig. 11), overprinting relations and nature of associated rocks (blueschist and/or greenschist-facies metabasalts and clastic metasediments), the development of the above-characterized microstructural Groups 1–3 is interpreted in the context of regional tectono-metamorphic events.

Group 1 microstructure (Fig. 10) is associated with large columnar calcite grains that are commonly interpreted to originate from back-reaction of HP aragonite to calcite (e.g., Brady et al. 2004; Seaton et al. 2009; Gerogiannis et al. 2021; Aravadinou et al. 2022). For this reason, the G1A microstructure in the studied metacarbonates is interpreted to reflect deformation D1 related to subduction of the Meliatic oceanic lithosphere (e.g., Dallmeyer et al. 2008; Plašienka et al. 2019). High-grade microstructure of the sampled G1 metacarbonates is corroborated by locally intercalating basic volcanics or volcanoclastics with relics of blueschist-facies minerals (e.g., Faryad 1995a, b; Mello et al. 1998; Ivan and Méres 2009; Plašienka et al. 2019).

The sampled G1 metacarbonates thus further constrain the extent of the HP Bôrka Nappe in the central and eastern part of the studied area at the northern edge of the Slovak Karst Mts and in the Nižná Slaná Depression (Fig. 11). Maximum P–T conditions in the glaucophanized metabasalts, as well as in clastic metasediments, were estimated to 400–460 °C at 1–1.2 GPa (Faryad 1995a, b, 1999; Faryad and Henjes-Kunst 1997). However, recent thermobarometric modeling concluded even higher P–T conditions reaching the eclogite-facies stability field at 520 °C and 1.55 GPa (Nemec et al. 2020). The lobate calcite grains of G1B microstructure, which do not contain relics of columnar calcite, indicate relatively high temperature deformation that may correspond to the initial phase of exhumation from the subduction channel (see below).

The Bôrka Nappe is currently located in the footwall of massive Triassic complexes of the Silica Nappe and in the hanging wall of the Gemic Unit as a result of its subsequent exhumation/emplacement deformation D2. In the studied metacarbonates, this deformation is likely associated with recrystallization of G1 microstructure and development of fine-grained G2 microstructure (Fig. 7). Spatial coincidence of G1 and G2 microstructures (Fig. 11) reflects the development of G2–D2 anastomosing mylonite shear zones surrounding the G1–D1 low-strain domains. Analogously,

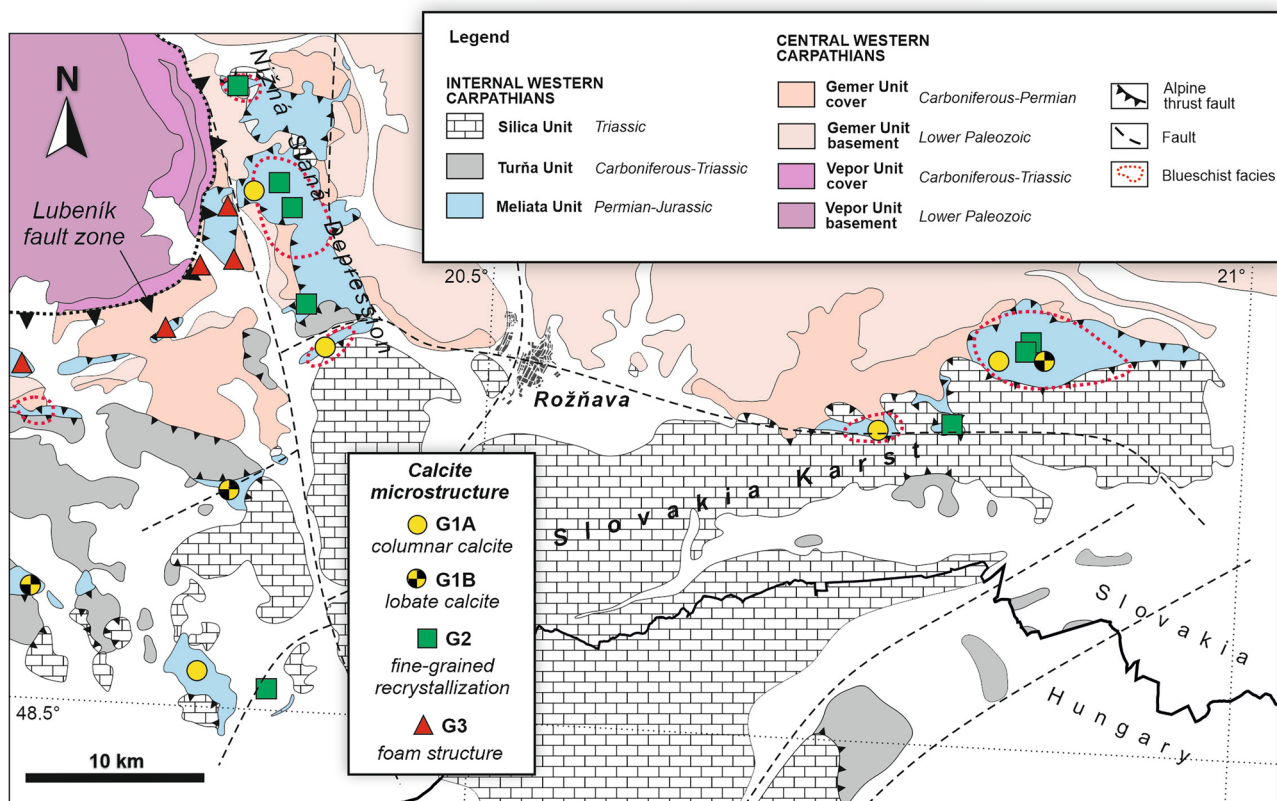


Fig. 11 Tectonic map of investigated area (modified after Bezák et al. 2004), with distribution of characteristic microstructures of metacarbonates. Note that the area with occurrence of G3 microstructures

should be re-interpreted as a distinct Vepor–Gemer contact zone, but it has not been regionally constrained yet

the better preserved HP–LT metamorphic assemblages (D1) in the blueschists correspond to low-strain domains of the D2 phase, while they are intensely overprinted by the greenschist-facies retrogression expressed as high-strain G2 calcite mylonites (Fig. 3b). Therefore, the blueschist to greenschist-facies transition determined from metabasites (Faryad 1999; Faryad et al. 2004; Dallmeyer et al. 2008) constrain also the P–T conditions of G1 to G2 microstructural transition (Fig. 10). In addition, the occurrence of G2 mylonites marks zones of intense shearing during exhumation and incorporation of the studied marbles into the accretionary wedge and/or thrusting over the Gemic substratum.

It should be mentioned that the subduction-related Group 1 microstructures occur also in marble blocks (Fig. 11) embedded in the deep marine low-grade metamorphosed Jurassic shales of the Meliata Unit s.s. (Árkai et al. 2003; Kövér et al. 2009). These were commonly interpreted as olistoliths (e.g., Mock et al. 1998), but their considerably higher degree of recrystallization/metamorphism with respect to the surrounding sediments indicates that they rather represent blocks tectonically separated from the underlying Bôrka Unit and incorporated within the low-grade matrix deposits that was associated with the development of an accretionary

complex. Due to their location in the low-grade fine-grained sediments, which accommodated most of the ductile deformation, the early G1 microstructure in these blocks was protected from significant later overprinting. With this respect only two samples (HCN5, BOH1 Table 1) showed pronounced foliation and lineation associated with the development of G2 microstructure during D2 deformation. The microstructural record revealed in studied blocks is thus similar to the Franciscan Complex in the North America where high-grade metamorphosed blocks are mixed with in low-grade or unmetamorphosed matrix (Wakabayashi 2015). On the other hand, the observed D2 structures may reflect later deformation associated with thrusting of the Meliata subduction–accretionary complex over the Gemic basement.

The occurrence of Group 3 microstructure is confined to the vicinity of the Lubeník shear zone (Fig. 11) marking the major tectonic contact between the Gemic and Veporic units (e.g., Novotná et al. 2015 and reference therein). This microstructure, characterized by uniform grain size and polygonal structure, is difficult to relate to the G1 and G2 microstructures (Fig. 10). In general, there are two possibilities: (1) G3 represents an event of static recrystallization related to the elevated temperatures in the vicinity of the

exhumed Veporic metamorphic dome, or (2) *G3* microstructure is not related to deformation of the Meliata Unit. As the grain size of *G3* microstructure is smaller than that of *G1* (Fig. 6), the formation of *G3* from *G1* by static recrystallization is not likely. Although it is possible that *G3* formed by static overprint of the finer-grained *G2*, the contrasting bright cathodoluminescence for *G2* and dark for *G3* (cf. Fig. 8c–f) makes this interpretation also unlikely. Therefore, the lack of overprinting relations and coherent appearance of *G3* microstructures only next to the Lubenik fault zone together with the lack of blueschist-facies metamorphic rocks in this region suggest that *G3* metacarbonates probably do not belong to the Meliata Unit. This conclusion is in agreement with opinions of some previous authors proposing that metacarbonates to the south of the Lubenik fault zone belong to the Carboniferous sedimentary complex of the Gemer Unit (Fusán 1957; Abonyi 1970; Gazdačko 2005) that was deformed during the Cretaceous juxtaposition of the Gemeric and Veporic Units (e.g., Novotná et al. 2015).

CPO data and orientation of lineation

Despite microstructural differences between the three groups, the observed calcite CPOs in most analyzed samples show maxima of *c*-axes and *e*-axes perpendicular to the measured foliation and maxima of *a*-axes parallel to the measured lineation (Figs. 5, 8, 9). Such textures can be interpreted as a result of twinning + intracrystalline slip (e.g., Wenk et al. 1987; Bestmann et al. 2000). The *e*-twinning is corroborated by distribution of poles to *e*-planes perpendicular to foliation. The intracrystalline slip is likely dominated by basal $\langle a \rangle$ slip with some contribution of rhombic $\langle a \rangle$ slip (Schmid et al. 1987; De Bresser 1991; Bestmann et al. 2000). The activity of such slip systems results in concentration of *a*-axes subparallel to lineation. However, in some of the studied samples the maximum of *a*-axes is oblique or even perpendicular to the measured lineation implying wrong kinematic section. For this reason, the resulting CPOs were rotated around the axis perpendicular to the foliation, so that the maximum concentration of *a*-axes is located at the periphery of pole figures (Fig. 12a–d). The rotations led to correction of kinematic sections which consequently allowed for correction of field lineation measurements for samples ROS1, HR9, BOR1 and VC29. An incorrect determination of the stretching lineation in the field is probably related to its weak character, as well as to a possible overprint during later low-grade deformation. The orientation of stretching lineation evaluated from calcite CPOs shows generally E–W to SE–NW trends which slightly contrasts with the E- to S-plunging lineation spread measured in the field (cf. Figs. 13, 2c).

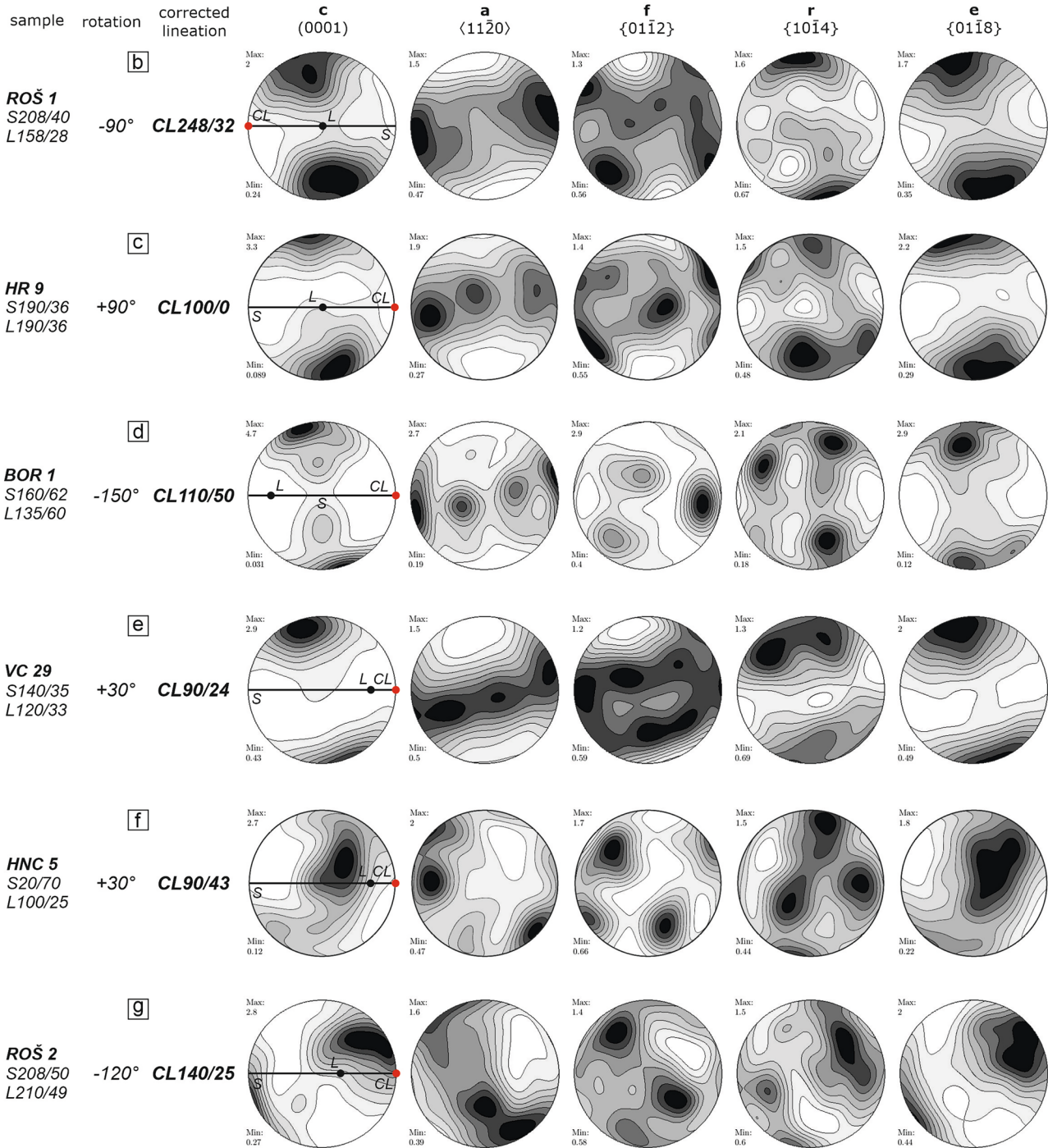
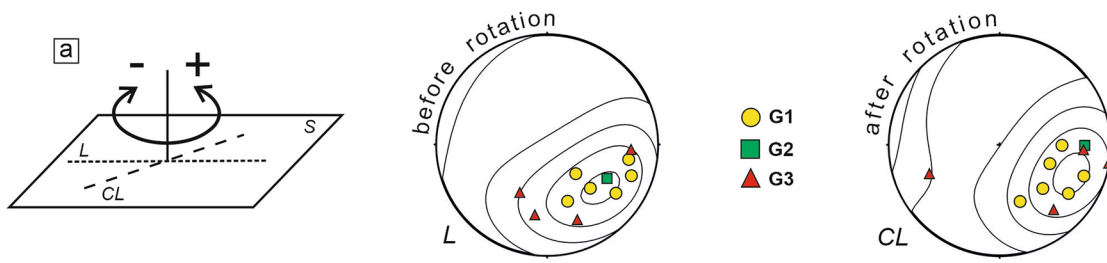
The observed CPOs in samples HCN5 and ROS2 (Figs. 5i, 8g) show a more complicated texture with the

maximum of *c*-axis subparallel to the measured lineation and a girdle of *a*-axes subperpendicular to foliation. Similar texture had been previously reported from deformation experiments on the fine-grained Solnhofen limestone and interpreted as a result of grain boundary sliding with minor contribution of *f*-slip (Schmid et al. 1987). Such interpretation, however, does not comply with the relatively large grain size observed in both samples that would likely prevent the grain boundary sliding mechanism. It seems more likely that the observed CPOs in HCN5 and ROS2 samples reflect wrong kinematic sections. In the light of the prevailing E–W kinematic sections for most of the studied samples, the CPOs of these two samples were tentatively rotated into the E–W-trending section (Fig. 12f, g). Although the rotated CPOs are still not ideal, they are much more coherent with textures recorded by the other samples. For this reason, the corrected lineation of the two samples has also been plotted into stereograms in Fig. 12.

Deformation history of the Meliata subduction-accretionary complex

The time of the HP–LT metamorphism in the Bôrka Nappe is constrained by the K–Ar and $^{40}\text{Ar}/^{39}\text{Ar}$ data. Dallmeyer et al. (1996, 2008) reported plateau ages between 150 and 160 Ma from clastic sediments of the lower complex. Plateau ages of phengite from phyllites and impure marbles provided 155–152 Ma (Maluski et al. 1993; Faryad and Henjes-Kunst 1997). However, older ages below 160–170 Ma were also detected. The electron microprobe analyzer (EMPA) monazite age spectra vary in a wide range, but ages up to 180 Ma are common (Vozárová et al. 2014; Plašienka et al. 2019; Potočný 2021; Potočný et al. 2020; Fig. 13). These data indicate that the deepest burial and subduction-related metamorphic peak of Bôrka Nappe complexes occurred during the Late Jurassic, just before the onset of exhumation. Scarce older ages admit the Early Jurassic commencement of the “Meliata Ocean” subduction, which is indicated also by the sedimentary record (start of the flysch-type sedimentation, e.g., Kozur 1991).

Lineations from the Group 1 samples likely correspond to D1 deformation in the subduction channel at peak metamorphic conditions and/or during the early exhumation. The corrected orientation of the *G1* stretching lineation revealed E–SE plunges determined in this work (Fig. 13), and differs from S to SE plunges of macroscopic lineation reported by Dallmeyer et al. (2008). The kinematic continuity of subduction–exhumation process is reflected by D2 shearing and development of Group 2 microstructures associated with E-plunging lineation (Fig. 12). D2 shearing was concentrated to comparatively weaker rocks like phyllites and impure limestones, particularly at the base and within the Meliata complex. West- to NW-facing recumbent



◀**Fig. 12** Correction of lineation orientation: **a** lineations before and after correction; **b–g** pole figures show CPO after rotation plotted with respect to the sample reference frame (measurement of foliation S and lineation L), foliation trace S, lineation orientation L and corrected lineation CL (identical for all pole figures) is shown in the c-axis pole figure

isoclinal folds (Potočný 2021) with axial-planar cleavage and ESE plunging stretching lineation largely mimic D1 kinematic framework, but decreasing pressures and temperatures already indicate gradual exhumation and internal imbrication of the Bôrka Nappe. Preceding the closure of the “Meliata Ocean”, the ongoing shortening and possibly return flow in the subduction channel brought the Bôrka complexes to the sole of the upper-plate units consisting of the Meliatic ophiolitic mélanges, low-grade Jurassic flysch (Meliata Unit s.s.) and of the overlying Turňa Nappe. In time of the closing stage of the Meliata suture, all these units were mutually imbricated to form an amalgamated accretionary complex that was finally thrust over the lower plate CWC Gemer Unit (Fig. 1), see also Lačný et al. (2016). As revealed by the geochronological data, the early D2 thrusting event occurred during the earliest Cretaceous time (Fig. 13), approximately between 145 and 140 Ma (Plašienka 2018; Plašienka et al. 2019 and references therein).

After the closure of the “Meliata Ocean”, the deformation progressed to the Eo-Alpine convergence reflected by shortening of the lower plate Gemer Unit with the development of regional cleavage fan and its thrusting over the Veporic domain (e.g., Lexa et al. 2003; Jeřábek et al. 2012; Novotná et al. 2015). Thrusting was accompanied by crustal thickening and the first phase of extensional collapse of the upper parts of the thrust wedge built up mainly by the Meliatic accretionary complexes, described e.g., by Dallmeyer et al. (2008) as top-to-southeast simple shearing in calcitic mylonites. The associated greenschist-facies metamorphism in the Gemer Unit and topmost elements of the wedge (Meliata Unit s.s. and Turňa Unit), as well as the retrogression in the Bôrka Nappe, were dated as a long time span 150–110 Ma by Árkai et al. (2003), Dallmeyer et al. (2008), Hurai et al. (2008, 2015), Putiš et al. (2012, 2014), Vozárová et al. (2014), Li et al. (2014), Plašienka et al. (2019), Kiefer et al. (2020) and Potočný et al. (2020)—see Fig. 13.

Deformation history of the Gemer–Vepor contact zone

The Group 3 microstructures most likely reflect deformation during the Cretaceous juxtaposition between the Gemer and Vepor units. The corrected orientation of G3 stretching lineation revealed major shift from dominantly S-plunging field lineations to dominantly E–W-trending corrected stretching

directions (Fig. 12). Such orientations are in an excellent agreement with the generally E–W-trending stretching lineations of the underlying Vepor Unit (Hók et al. 1993; Plašienka 1993; Janák et al. 2001; Jeřábek et al. 2007, 2012; Bukovská et al. 2013; Novotná et al. 2015). These lineations are explained as orogen-parallel stretching of the underlying Vepor associated with northward overthrusting of the Gemer Unit (Jeřábek et al. 2007, 2012). The prograde subhorizontal deformation fabric associated with the lower crustal flow was followed by a static metamorphic overprint recorded namely in the kyanite-chloritoid schists of the Permian cover delineating the southern edge of the Veporic unit (Vrána 1964; Lupták et al. 2000; Novotná et al. 2015). The kyanite and chloritoid overgrowing the subhorizontal fabric were associated with growth of monazite dated by ICPMS to 97 ± 4 Ma (Bukovská et al. 2013; Jeřábek et al. 2012). The observed annealing of the G3 metacarbonates can be thus related to this postkinematic event, especially since recent EMPA dating of monazite in chlorite-sericite phyllites at the locality Hrádok (sampling site HR9) revealed dominant peak of ages at 97 ± 5 Ma (Plašienka et al. 2019). Consequently, the annealed microfabric observed in metacarbonates previously assigned to the Bôrka Nappe (Fig. 11) is apparently related to this event and thus should have not affected the Meliatic, but the lowermost Gemeric structural elements formed by Carboniferous, carbonate-bearing formations.

Conclusions

This work is devoted to microstructures of metacarbonates from the subduction–accretionary complex related to closure of the “Meliata Ocean”. Based on the observation of microstructures, the studied samples were divided into three groups that reflect different P–T–t–D evolution, and possibly also deformation stages as characterized below.

1. Deformation and metamorphism under conditions of high pressures (> 1 GPa) and medium-temperatures (< 500 °C) are expressed by columnar calcite preserved in metacarbonates of the Group 1 microstructure in the sliced Bôrka Nappe. G1 microstructure occurs in a direct contact with intercalated blueschists but also within metacarbonate bodies enclosed in weakly metamorphosed matrix sediments. G1 microstructure is associated with subduction of the Meliata oceanic lithosphere (D1) recorded in the Meliatic high-pressure Bôrka Nappe. The documentation of high-pressure marble blocks in the low-grade pelagic-clastic sediments of the Meliata Unit infers development of the Franciscan-type accretionary complex. The corrected orientation of lineations related to subduction–exhumation of the Meliata com-

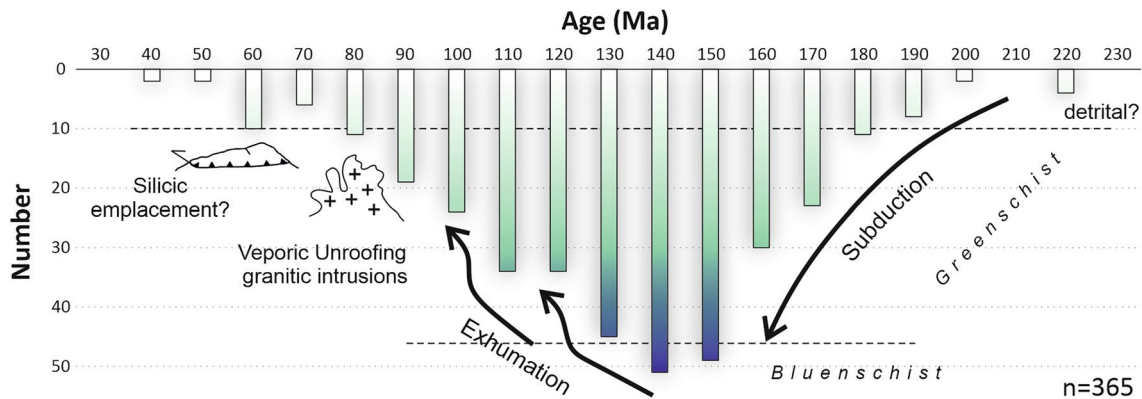


Fig. 13 U–Th–Pb monazite age spectra from the Bôrka Nappe according to Potočný (2021)

plex suggests top-to-WNW kinematics which contrasts with the previously proposed N–NW directions.

- The Group 2 microstructure indicates a lower temperature overprint of G1, which locally led to complete recrystallization of G1 and formation of calcitic mylonites in narrow shear zones. This deformation (D2) is associated with localization of deformation during exhumation of the Bôrka Nappe, as well as imbrication and splitting of the entire subduction–accretionary complex into several slices probably during their thrusting over the underlying Gemic units.
- The Group 3 microstructure is spatially restricted to the vicinity of the Lubeník fault zone separating the major Gemic and Veporic tectonic units. G3 microstructure shows evidence for static recrystallization that is difficult to relate to the G1–G2 microstructures of the Bôrka nappe. Instead, this microstructure likely reflects deformation during thrusting of the Gemic Unit over the Veporic Unit resulting in an E–W orogen-parallel stretching of the lower complexes and their subsequent static metamorphic overprint. The studied metacarbonates to the south of the Lubeník fault zone, formerly affiliated with the Bôrka Nappe, are thus re-interpreted as Carboniferous sedimentary complex of the Gemic Unit.

Acknowledgements Financial supports from the Slovak Research and Development Agency (projects APVV-17-0170 and APVV-21-0281), Grant Agency for Science, Slovakia, Agentúra Ministerstva Školstva, Vedy, Výskumu a Športu SR (project VEGA 1/0435/21) and National Scholarship Programme of the Slovak Republic are gratefully appreciated. We are thankful also to Marco Herwegh and Alfons Berger from the Institute of Geological Sciences of University Bern for valuable discussions and suggestions. An anonymous reviewer, Giancarlo Molli, László Fodor and editor-in chief Ulrich Riller are acknowledged for constructive remarks and suggestions that substantially improved the scientific level of the earlier versions of the manuscript.

Funding Open access funding provided by The Ministry of Education, Science, Research and Sport of the Slovak Republic in cooperation with Centre for Scientific and Technical Information of the Slovak Republic.

Data availability The authors confirm that the data supporting the findings of this study are available within the article.

Open Access This article is licensed under a Creative Commons Attribution 4.0 International License, which permits use, sharing, adaptation, distribution and reproduction in any medium or format, as long as you give appropriate credit to the original author(s) and the source, provide a link to the Creative Commons licence, and indicate if changes were made. The images or other third party material in this article are included in the article's Creative Commons licence, unless indicated otherwise in a credit line to the material. If material is not included in the article's Creative Commons licence and your intended use is not permitted by statutory regulation or exceeds the permitted use, you will need to obtain permission directly from the copyright holder. To view a copy of this licence, visit <http://creativecommons.org/licenses/by/4.0/>.

References

- Abonyi A (1970) Predbežné výsledky porovnávacieho štúdia stratigrafie a tektoniky severného pruhu karbónu gemicíd z oblasti Jelšavy a Dobšinej. *Miner Slov* 2:217–230
- Aravadinou E, Gerogiannis N, Xypolias P (2022) Development and passive exhumation of high-pressure shear zones (Blueschist Unit, Syros): Insights from quartz and columnar calcite microstructures. *J Struct Geol* 159:2–16
- Árkai P, Faryad SW, Vidal O, Balogh K (2003) Very low-grade metamorphism of sedimentary rocks of the Meliata unit, Western Carpathians, Slovakia: implications of phyllosilicate characteristics. *Int J Earth Sci* 92:68–85
- Bestmann M, Kunze K, Matthews A (2000) Evolution of a calcite marble shear zone complex on Thassos Island, Greece: microstructural and textural fabrics and their kinematic significance. *J Struct Geol* 22:1789–1807
- Bezák V (ed.), Broska I, Ivanička J, Reichwalder P, Vozár J, Polák M, Havrila M, Mello J, Biely A, Plašienka D, Potfaj M, Žec B, Vass D, Elečko M, Janočko J, Peresztlényi M, Marko F, Maglay J, Pristaš J (2004) Tectonic map of Slovak Republic 1: 500,000 with explanations. State Geological Institute of Dionyz Stur, Bratislava

- Brady JB, Markley MJ, Schumacher JC, Cheney JT, Bianciardi GA (2004) Aragonite pseudomorphs in high-pressure marbles of Syros, Greece. *J Struct Geol* 26:3–9
- Bukovská Z, Jeřábek P, Lexa O, Konopásek J, Janák M, Košler J (2013) Kinematically unrelated C–S fabrics: an example of extensional shear band cleavage from the Veporic Unit (Western Carpathians). *Geol Carpath* 64:103–116
- Burkhard M (1993) Calcite twins, their geometry, appearance and significance as stress–strain markers and indicators of tectonic regime: a review. *J Struct Geol* 15:351–368
- Channell JET, Kozur HW (1997) How many oceans? Meliata, Vardar and Pindos oceans in Mesozoic Alpine paleogeography. *Geology* 25:183–186
- Csontos L, Vörös A (2004) Mesozoic plate tectonic reconstruction of the Carpathian region. *Palaeogeogr Palaeoclimatol Palaeoecol* 210:1–56
- Dallmeyer RD, Neubauer F, Handler R, Fritz H, Müller W, Pana D, Putiš M (1996) Tectonothermal evolution of the internal Alps and Carpathians: evidence from $40\text{Ar}/39\text{Ar}$ mineral and whole-rock data. *Eclogae Geol Helv* 89:203–227
- Dallmeyer RD, Neubauer F, Fritz H (2008) The Meliata suture in the Carpathians: regional significance and implications for the evolution of high-pressure wedges within collisional orogens. In: Siegesmund S, Fügenschuh B, Froitzheim N (eds) *Tectonic aspects of the Alpine-Dinaride-Carpathian system*, vol 298. Geological Society, Special Publication, London, pp 101–115
- De Bresser H (1991) Intracrystalline deformation of calcite. Doctoral thesis, Utrecht University
- Ernst WG (1988) Tectonic history of subduction zones inferred from retrograde blueschist PT paths. *Geology* 16:1081–1084
- Faryad SW (1995a) Phase petrology and P–T conditions of mafic blueschists from the Meliata unit, West Carpathians, Slovakia. *J Metamorphic Geol* 13:701–714
- Faryad SW (1995b) Petrology and phase relations of low-grade high-pressure metasediments from the Meliata Unit (West Carpathians, Slovakia). *Eur J Miner* 7:71–87
- Faryad SW (1999) Exhumation of the Meliata high-pressure rocks (Western Carpathians): petrological and structural record in blueschists. *Acta Montan Slov* 4:137–144
- Faryad SW, Henjes-Kunst F (1997) Petrological and K–Ar and ^{40}Ar – ^{39}Ar age constraints for the tectonothermal evolution of the high-pressure Meliata unit, Western Carpathians (Slovakia). *Tectonophysics* 280:141–156
- Faryad SW, Hoinkes G (1999) Two contrasting mineral assemblages in the Meliata blueschists, Western Carpathians, Slovakia. *Mineral Mag* 63:489–501
- Faryad SW, Schulmann K, Lexa O (2004) Pre-conference fieldtrip: structure and metamorphism of the Meliata Unit. CETEG—2nd meeting of the Central European Tectonic Studies Group. *GeoLines* 17:111–120
- Faryad SW, Spišiak J, Horváth P, Hovorka D, Dianiška I, Józsa S (2005) Petrological and geochemical features of the Meliata mafic rocks from the sutured Triassic oceanic basin, Western Carpathians. *Ofioliti* 30:27–35
- Festa A, Pini GA, Dilek Y, Codegone G (2010) Mélanges and mélange-forming processes: a historical overview and new concepts. *Int Geol Rev* 52:1040–1105
- Fusán O (1957) Paleozoikum Gemeríd. *Geol Práce Zoš* 46:17–37
- Gazd'áčko Ľ (2005) Litologická náplň a vzťah bôrčanského príkrovu v okolí Markušky a Kobeliarova k ultrabázikám. *Miner Slov* 37:214–217
- Gerogiannis N, Aravadinou E, Chatzaras V, Xypolias P (2021) Calcite pseudomorphs after aragonite: a tool to unravel the structural history of high-pressure marbles (Evia Island, Greece). *J Struct Geol* 148:1–16
- Gy L (2000) Polyphase structural evolution of the Aggtelek-Rudabánya Mountains (NE Hungary), the southernmost element of the Inner Western Carpathians—a review. *Slov Geol Mag* 6:260–268
- Haas J, Kovács S, Krystyn L, Lein R (1995) Significance of Late Permian-Triassic facies zones in terrane reconstructions in the Alpine-North Pannonian domain. *Tectonophysics* 242:19–40
- Herwegh M, Berger A (2004) Deformation mechanisms in second-phase affected microstructures and their energy balance. *J Struct Geol* 26:1483–1498
- Herwegh M, Kunze K (2002) The influence of nano-scale second-phase particles on deformation of fine grained calcite mylonites. *J Struct Geol* 24:1463–1478
- Herwegh M, Pfiffner OA (2005) Tectono-metamorphic evolution of a nappe stack: a case study of the Swiss Alps. *Tectonophysics* 404:55–76
- Hielscher R, Schaeben H (2008) A novel pole figure inversion method: Specification of the MTEX algorithm. *J Appl Crystallogr* 41:1024–1037
- Hók J, Kováč P, Madarás J (1993) Extenzná tektonika západného úseku styčnej zóny gemerika a veporika. *Miner Slov* 25:172–176
- Hsü KJ (1968) The principles of melanges and their bearing on the Franciscan–Knoxville paradox. *Geol Soc Am Bull* 79:1063–1074
- Hsü KJ (1974) Melanges and their distinction from olistostromes. In: Dott RHH, Shaver RH (eds) *Modern and ancient geosynclinal sedimentation*. Special publication of the Society of Economic Paleontologists and Mineralogists, Tulsa, pp 321–333
- Hurai V, Lexa O, Schulmann K, Montigny R, Prochaska W, Frank W, Konečný P, Král J, Thomas R, Chovan M (2008) Mobilization of ore fluids during Alpine metamorphism: evidence from hydrothermal veins in the Variscan basement of Western Carpathians, Slovakia. *Geofluids* 8:181–207
- Hurai V, Paquette JL, Lexa O, Konečný P, Dianiška I (2015) U–Pb–Th geochronology of monazite and zircon in albitite metasomatites of the Rožňava–Nadabula ore field (Western Carpathians, Slovakia): implications for the origin of hydrothermal polymetallic siderite veins. *Miner Petrol* 109:519–530
- Ivan P (2002) Relics of the Meliata Ocean crust: geodynamic implications of mineralogical, petrological and geochemical proxies. *Geol Carpath* 53:245–256
- Ivan P, Méres Š (2009) Enkláva metamorfitu fácie modrých bridlíc v došbinskom serpentinitovom lome – dôkaz spojitosti ultrabázického telesa s hačavskou formáciou príkrovu Bôrky. *Miner Slov* 41:407–418
- Ivan P, Méres Š, Sýkora M (2009) Magnezioriebeckit v červených silicích a bazaltoch z Jakloviec—indikátor iniciálneho štádia vysokotlakovej subdukčnej metamorfózy. *Miner Slov* 41:419–432
- Janák M, Plašienka D, Frey D, Cosca M, Schmidt ST, Lupták B, Méres Š (2001) Cretaceous evolution of a metamorphic core complex, the Veporic unit, Western Carpathians (Slovakia): P–T conditions and in situ $^{40}\text{Ar}/^{39}\text{Ar}$ UV laser probe dating of metapelites. *J Metamorph Geol* 19:197–216
- Jeřábek P, Stünitz H, Heilbronner R, Lexa O, Schulmann K (2007) Microstructural-deformation record of an orogen-parallel extension in the Veporic Unit, West Carpathians. *J Struct Geol* 29:1722–1743
- Jeřábek P, Lexa O, Schulmann K, Plašienka D (2012) Inverse ductile thinning via lower crustal flow and fold-induced doming in the West Carpathian Eo-Alpine collisional wedge. *Tectonics* 31:TC5002
- Kiefer S, Števkó M, Vojtko R, Ozdín D, Gerdes A, Creaser RA, Szczerba M, Majzlan J (2020) Geochronological constraints on the carbonate-sulfarsenide veins in Dobšiná, Slovakia: U/Pb ages of hydrothermal carbonates, Re/Os age of gersdorffite, and K/Ar ages of fuchsite. *J Geosci* 65:229–247

- Kovács S (1992) Tethys “western ends” during the Late Paleozoic and Triassic and their possible genetic relationships. *Acta Geol Hung* 35:329–369
- Kövéř S, Fodor L, Judik K, Németh T, Balogh K, Kovács S (2009) Deformation history and nappe stacking in Rudabánya Hills (Inner Western Carpathians) unravelled by structural geological, metamorphic petrological and geochronological studies of Jurassic sediments. *Geodin Acta* 22:3–29
- Kövéř S, Fodor L, Kovács Z, Klötzli U, Haas J, Zajcon N, Cs S (2018) Late Triassic acidic volcanic clasts in different Neotethyan sedimentary mélanges: paleogeographic and geodynamic implications. *Int J Earth Sci* 107:2975–2998
- Kozur H (1991) The evolution of the Meliata-Hallstatt ocean and its significance for the early evolution of the Eastern Alps and Western Carpathians. *Palaeogeogr Palaeoclimatol Palaeoecol* 87:109–135
- Kozur H, Mock R (1973) Zum Alter und zur tektonischen Stellung der Meliata-Serie des Slowakischen Karstes. *Geol Carpath* 24:365–374
- Lačný A, Plašienka D, Vojtko R (2016) Structural evolution of the Turňa Unit constrained by fold and cleavage analyses and its consequences for the regional tectonic models of the Western Carpathians. *Geol Carpath* 67:177–193
- Lexa O, Schulmann K, Ježek J (2003) Cretaceous collision and indentation in the West Carpathians: view based on structural analysis and numerical modeling. *Tectonics* 22:1066
- Li XH, Putiš M, Yang YH, Koppa M, Dyda M (2014) Accretionary wedge harzburgite serpentinization and rodingitization constrained by perovskite U/Pb SIMS age, trace elements and Sm/Nd isotopes: case study from the Western Carpathians, Slovakia. *Lithos* 205:1–14
- Lupták B, Janák M, Plašienka D, Schmidt ST, Frey M (2000) Chloritoid-kyanite schists from the Veporic unit, Western Carpathians, Slovakia: implications for Alpine (Cretaceous) metamorphism. *Schweiz Mineral Petrogr Mitt* 80:213–223
- Maluski H, Rajlich P, Matte P (1993) ^{40}Ar – ^{39}Ar dating of the Inner Carpathians Variscan basement and Alpine mylonitic overprinting. *Tectonophysics* 225:313–337
- Mello J (1975) Pelagic and reef sediment relations of the Middle Triassic in the Silica nappe and transitional strata nature (the Slovak Karst, West Carpathians). *Geol Zbor Geol Carpath* 26:237–252
- Mello J, Reichwalder P, Vozárová A (1998) Bôrka Nappe: high-pressure relic from the subduction-accretion prism of the Meliata ocean (Inner Western Carpathians, Slovakia). *Slov Geol Mag* 4:261–273
- Missoni S, Gawlick HJ (2011) Jurassic mountain building and Mesozoic-Cenozoic geodynamic evolution of the Northern Calcareous Alps as proven in the Berchtesgaden Alps (Germany). *Facies* 57:137–186
- Mock R, Sýkora M, Aubrecht R, Ožvoldová L, Kronome B, Reichwalder P, Jablonský J (1998) Petrology and stratigraphy of the Meliaticum near the Meliata and Jaklovce villages, Slovakia. *Slov Geol Mag* 4:223–260
- Nemec O, Putiš M, Bačík P, Ružička P, Németh Z (2020) Metamorphic conditions of Neotethyan Meliatic accretionary wedge estimated by thermodynamic modelling and geothermobarometry (Inner Western Carpathians). *Minerals* 10:1094
- Novotná N, Jeřábek P, Pitra P, Lexa O, Racek M (2015) Repeated slip along a major decoupling horizon between crustal-scale nappes of the Central Western Carpathians documented in the Ochtiná tectonic mélange. *Tectonophysics* 646:50–64
- Oesterling N, Heilbronner R, Stünitz H, Barnhoorn A, Moll G (2007) Strain dependent variation of microstructure and texture in naturally deformed Carrara marble. *J Struct Geol* 29:681–696
- Plašienka D (1993) Structural pattern and partitioning of deformation in the Veporic Foederata cover unit (Central Western Carpathians). In: Rakús M, Vozár J (eds) *Geodynamic model and deep structure of the Western Carpathians*. Geological Institute of Dionýz Štúr, Bratislava, pp 269–277
- Plašienka D (2018) Continuity and episodicity in the early Alpine tectonic evolution of the Western Carpathians: how large-scale processes are expressed by the orogenic architecture and rock record data. *Tectonics* 37:2029–2079
- Plašienka D, Méřes Š, Sýkora M, Soták J, Lačný A, Aubrecht R, Bellová S, Potočný T (2019) Meliatic blueschists and their detritus in Cretaceous sediments: new data constraining tectonic evolution of the West Carpathians. *Swiss J Geosci* 112:55–81
- Potočný T, Méřes Š, Plašienka D (2020) Geological structure and tectonometamorphic evolution of the Veporic-Gemeric contact zone constrained by the monazite age data (Slavošovce–Štítnik area, Western Carpathians, Slovakia). *Miner Slov* 52:83–102
- Potočný T (2021) *Tektonometamorfný vývoj meliatického príkrovu Bôrky a jeho vzťahy k okolitým jednotkám*. Department of Geology and Paleontology, Dissertation thesis
- Putiš M, Frank W, Plašienka D, Siman P, Sulák M, Biroň A (2009) Progradation of the Alpidic Central Western Carpathians orogenic wedge related to two subductions: constrained by $^{40}\text{Ar}/^{39}\text{Ar}$ ages of white micas. *Geodin Acta* 22:31–56
- Putiš M, Radvanec M, Sergeev S, Koller F, Michálek M, Snárska B, Koppa M, Šarinová K, Németh Z (2011) Metamorfovaná sukcesia silicitických bridlíc s bazaltom a diastróficou brekciou v olistolite jurskej akrečnej prizmy meliatika pri Jaklovciach (Slovensko), datovaná na zirkón (U-Pb SIMS SHRIMP). *Miner Slov* 43:1–18
- Putiš M, Koppa M, Snárska B, Koller F, Uher P (2012) The blueschist-associated perovskite-andradite-bearing serpentinized harzburgite from Dobšiná (the Meliata Unit), Slovakia. *J Geosci* 57:221–240
- Putiš M, Danišík M, Ružička P, Schmiedt I (2014) Constraining exhumation pathway in accretionary wedge by (U-Th)/He thermochronology—case study on Meliatic nappes in the Western Carpathians. *J Geodyn* 81:80–90
- Putiš M, Yang YH, Koppa M, Dyda M, Šmál P (2015) U/Pb LA-ICP-MS age of metamorphic-metasomatic perovskite from serpentinized harzburgite in the Meliata Unit at Dobšiná, Slovakia: Time constraints of fluid-rock interaction in an accretionary wedge. *Acta Geol Slov* 7:63–71
- Putiš M, Soták J, Li QL, Ondrejka M, Li XH, Hu Z, Ling X, Nemeč O, Németh Z, Ružička P (2019) Origin and age determination of the Neotethys Meliata Basin ophiolite fragments in the Late Jurassic–Early Cretaceous accretionary wedge mélange (Inner Western Carpathians, Slovakia). *Minerals* 9(11):652
- Rakús M (1996) Jurassic of the innermost Western Carpathians zones—its importance and influence on the geodynamic evolution of the area. *Slov Geol Mag* 3–4(96):311–317
- Reichwalder P (1982) Structural characteristic of root zones of some nappes in innermost parts of West Carpathians. In: Mahef M (ed) *Alpine structural elements: Carpathian–Balkan–Caucasus–Pamir orogene zone*, pp 43–56
- Rogowitz A, Grasemann B, Huet B, Habler G (2014) Strain rate dependent calcite microfabric evolution—an experiment carried out by nature. *J Struct Geol* 69(part A):1–17
- Schmid SM, Panozzo R, Bauer S (1987) Simple shear experiments on calcite rocks: rheology and microfabric. *J Struct Geol* 9:747–778
- Schmid SM, Bernoulli D, Fügenschuh B, Matenco L, Schefer S, Schuster R, Tischler M, Ustaszewski K (2008) The Alpine–Carpathian–Dinaridic orogenic system: correlation and evolution of tectonic units. *Swiss J Geosci* 101:139–183
- Seaton NCA, Whitney DL, Teyssier Ch, Toraman E, Heizler MT (2009) Recrystallization of high-pressure marble (Sivrihisar, Turkey). *Tectonophysics* 479:241–253
- Stampfli GM, Kozur HW (2006) Europe from Variscan to the Alpine cycles. *Geol Soc Lond Mem* 32:57–82

- Szives O, Fodor L, Fogarasi A, Sz K (2018) Integrated calcareous nannofossil and ammonite data from the upper Barremian–lower Albian of the northeastern Transdanubian Range (central Hungary): stratigraphical implications and consequences for dating tectonic events. *Cretaceous Res* 91:229–250
- Vojtko R, Králiková S, Jeřábek P, Schuster R, Danišík M, Fügenschuh B, Minár J, Madarás J (2016) Geochronological evidence for the Alpine tectono-thermal evolution of the Veporic Unit (Western Carpathians, Slovakia). *Tectonophysics* 666:48–65
- Vozárová A (1996) Tectono-sedimentary evolution of Late Paleozoic basins based on interpretation of lithostratigraphic data (Western Carpathians; Slovakia). *Slovak Geol Mag* 3–4(96):251–271
- Vozárová A, Vozár J (1988) Late Paleozoic in the West Carpathians. Geologický ústav Dionýza Štúra, Bratislava
- Vozárová A, Konečný P, Šarinová K, Vozár J (2014) Ordovician and Cretaceous tectonothermal history of the Southern Gemericum Unit from microprobe monazite geochronology (Western Carpathians, Slovakia). *Int J Earth Sci* 103:1005–1022
- Vozárová A, Radionov N, Šarinová K, Lepekhina E, Vozár J, Paderin I (2019) Detrital zircon U–Pb geochronology of Pennsylvanian–Permian sandstones from the Turnaicum and Meliaticum (Western Carpathians, Slovakia): provenance and tectonic implications. *Int J Earth Sci* 108:1793–1815
- Vrána S (1964) Chloritoid and kyanite zone of alpine metamorphism on the boundary of the Gemericides and Veporides (Slovakia). *Kryštalínium* 2:125–143
- Wakabayashi J (2015) Anatomy of a subduction complex: architecture of the Franciscan Complex, California, at multiple length and time scales. *Int Geol Review* 57:669–746
- Walker G, Burley S (1991) Luminescence petrography and spectroscopic studies of diagenetic minerals. In: Barker CE, Kopp OC (eds) *Luminescence microscopy and spectroscopy: qualitative and quantitative applications*. SEMP Short Course, vol 25, pp 83–96
- Wenk HR, Takeshita T, Bechler E, Erskine BG, Matthies S (1987) Pure shear and simple shear calcite textures. Comparison of experimental, theoretical and natural data. *J Struct Geol* 9:731–745